PNNL-28427

Pacific Northwest
NATIONAL LABORATORY

Evaluation of Nondestructive Examination Responses from Chloride-Induced Stress Corrosion Cracks

Fabrication of Base Metal Test Specimens

September 2019

RM Meyer
SG Pitman
MR Larche
MS Prowant
ME Dahl
JD Suter
KF Mattlin

Prepared for the U.S. Nuclear Regulatory Commission
under a Related Services Agreement with the U.S. Department of Energy
CONTRACT DE-AC05-76RL01830

U.S. DEPARTMENT OF ENERGY

DISCLAIMER

PACIFIC NORTHWEST NATIONAL LABORATORY
operated by
BATTELLE
for the
UNITED STATES DEPARTMENT OF ENERGY
under Contract DE-AC05-76RL01830

Printed in the United States of America

Available to DOE and DOE contractors from the
Office of Scientific and Technical Information,
P.O. Box 62, Oak Ridge, TN 37831-0062;
ph: (865) 576-8401
fax: (865) 576-5728
email: reports@adonis.osti.gov

Available to the public from the National Technical Information Service,
U.S. Department of Commerce, 5285 Port Royal Rd., Springfield, VA 22161
ph: (800) 553-6847
fax: (703) 605-6900
email: orders@ntis.fedworld.gov
online ordering: http://www.ntis.gov/ordering.htm

This document was printed on recycled paper.
(9/2003)

PNNL-28427

Evaluation of Nondestructive Examination Responses from Chloride-Induced Stress Corrosion Cracks

Fabrication of Base Metal Test Specimens

September 2019

RM Meyer
SG Pitman
MR Larche
MS Prowant
ME Dahl
JD Suter
KF Mattlin

Prepared for
the U.S. Nuclear Regulatory Commission
under a Related Services Agreement
With the U.S. Department of Energy
Contract DE AC05 76RL01830

Pacific Northwest National Laboratory
Richland, Washington 99352

Executive Summary

This report documents efforts to create actual chloride-induced stress corrosion cracks (CISCCs) in stainless-steel specimens for evaluating application of nondestructive examination (NDE) technologies for detection and sizing of CISCC in stainless-steel canisters in dry storage systems (DSSs) for spent nuclear fuel. In the United States, several DSSs for commercial spent nuclear fuel are approaching the end of their initial licensed or certified term. Many of these systems were originally licensed or certified for 20 years, after which the licensing or certification may be renewed for periods up to 40 years, according to Title 10 of *the Code of Federal Regulations* (10 CFR), Part 72, "Licensing Requirements for the Independent Storage of Spent Nuclear Fuel, High-Level Radioactive Waste, and Reactor-Related Greater than Class C Waste." Guidance for review of renewal applications is provided in NUREG-1927, *Standard Review Plan for Renewal of Spent Fuel Dry Cask Storage System Licenses and Certificates of Compliance*. A review of aging effects that could affect important-to-safety structures, systems, and components is required in renewal applications and applicants are required to address aging effects using either a time-limited aging analysis or an aging management program. The U.S. Nuclear Regulatory Commission (NRC) issued NUREG-2214, *Managing Aging Processes In Storage (MAPS) Report*, which provides guidance on the evaluation of known aging degradation mechanisms to determine if they could affect the ability of dry storage system components to fulfill their safety functions in the 20- to 60-year period of extended operation.

In the United States, the majority of DSSs can be referred to as welded canister systems. These systems typically consist of a stainless-steel shell into which the spent fuel is loaded prior to sealing by welding. The welded canisters are then placed into a thick concrete overpack that provides physical protection for the welded canister and serves to shield the radiation emanating from the spent fuel. Concern regarding the potential degradation of welded canisters by CISCC were originally communicated by the NRC in a technical report (*Identification and Prioritization of the Technical Information Needs Affecting Potential Regulation of Extended Storage and Transportation of Spent Nuclear Fuel*) and in NRC Information Notice 2012-20 titled, "Potential Chloride-Induced Stress Corrosion Cracking of Austenitic Stainless Steel and Maintenance of Dry Cask Storage System Canisters." Although sheltered by the concrete overpack, welded canisters are still susceptible to exposure to chlorides and moisture that is carried by circulating air flow through ventilations in the overpack.

The potential for CISCC of DSSs is expected to be limited to locations with environments that contain significant chloride concentrations, high temperatures, and high humidity. However, the ability to detect and characterize potential flaws is an important consideration for future aging management activities. The response of an NDE technology to a flaw depends on several factors related to the flaw size, shape, and morphology. The objective of this effort is to create actual CISCCs in stainless-steel specimens so that the responses of NDE technologies can be evaluated using flaws with features (i.e., geometry and morphology) that are relevant to potential CISCC of stainless-steel canisters in DSSs for spent nuclear fuel.

The approach to producing desired specimens incorporated a "scoping" phase in which attempts at growing CISCCs were performed using a smaller test rig and smaller test specimens. The scoping phase was necessary to explore test parameters and practical aspects of design through trial-and-error. After achieving satisfactory results in the scoping phase, the manufacture of the final NDE specimens in the full-scale test rig could begin with confidence. The approach for fabricating flaws in both the scoping phase and for production of final NDE specimens may be characterized as "cook-and-look." While such an approach may lack the precision and level of control offered by a highly instrumented test setup, the "cook-and-look" approach is adequate for creating NDE specimens.

The scoping phase helped identify practical improvements to the test setup and suitable accelerated test parameters for initiating and growing large cracks in time intervals of one week or less.

Practical improvements identified through the scoping phase included:

- Replacing the PVC (polyvinyl chloride) cup for the $MgCl_2 \cdot 6H_2O$ (magnesium chloride hexahydrate) solution with a CPVC (chlorinated polyvinyl chloride) cup
- Reorienting the test rig so that the $MgCl_2 \cdot 6H_2O$ solution contacted the specimen from the side instead of from underneath
- Replacing the original polyamide mask material with a high-temperature engine enamel
- Adjusting the length of the mask penetration to control crack aspect ratio.

Suitable test parameters identified through the trial-and-error scoping phase are:

- Sensitizing the 304 stainless-steel specimens by soaking in a furnace for 40 hours at 600°C
- $MgCl_2 \cdot 6H_2O$ solution concentration of 6 mol/L or greater
- $MgCl_2 \cdot 6H_2O$ solution heated to 108°C.

By the end of the scoping phase, the ability to generate cracks with varying depths (i.e., 25%–75% through thickness) and with small crack opening displacement (approx. 10 µm) was demonstrated. Also, an ability to control the location of crack initiation was achieved by the application of the high-temperature enamel mask. Finally, an ability to control crack aspect ratio was shown through modification of the length of penetration through the mask.

Two NDE specimens were fabricated following the scoping phase of testing. The first NDE specimen was cautiously removed after a day of exposure to examine crack formation. An automated ultrasonic testing (UT) examination was unable to identify a crack tip signal suggesting the flaw is shallow (< 2 mm–3 mm). As is, this specimen can be useful in testing the ability of NDE technologies to detect cracks at early stages of growth and distinguishing technologies that exhibit exceptional detection and depth sizing capabilities. A second NDE specimen was fabricated to grow a crack with greater depth. In this case, the specimen was initially exposed for 30 hours and exposed again for another 24 hours. Following these exposures, a crack with depth of 8 mm (0.31 in.) was observed and estimated based on automated UT measurements. The testing performed in these efforts focused on specimens consisting only of base material. In the field, the concern with CISCC is focused on heat-affected-zones near welds. A suggested follow-on step to these efforts is to fabricate flaws in welded specimens.

Acknowledgments

This work was performed with Contracting Officer Representative oversight provided by Bruce Lin of the U.S. Nuclear Regulatory Commission (NRC). Additional technical direction and oversight was provided by Darrell Dunn, Matthew Hiser, and Margaret Audrain of the NRC. The authors would like to thank Ms. Kay Hass for formatting and editing this document.

Acronyms and Abbreviations

ASME	American Society of Mechanical Engineers
B&PV	Boiler and Pressure Vessel (Code)
CISCC	chloride-induced stress corrosion cracks
CoC	certificate of compliance
COD	crack opening displacement
CPVC	chlorinated polyvinyl chloride
DSS	dry storage systems
ECT	eddy current testing
EPRI	Electric Power Research Institute
HAZ	heat-affected-zones
$MgCl_2 \cdot 6H_2O$	magnesium chloride hexahydrate
NDE	nondestructive examination
NPP	nuclear power plant
NRC	U.S. Nuclear Regulatory Commission
PVC	polyvinyl chloride
SCC	stress corrosion crack
UT	ultrasonic testing
VT	visual testing

Contents

Figures

Tables

1.0 Introduction

This report documents efforts to create actual chloride-induced stress corrosion cracks (CISCCs) in stainless-steel specimens for evaluating application of nondestructive examination (NDE) technologies for detection and sizing of CISCC in stainless-steel canisters in dry storage systems (DSSs) for spent nuclear fuel. In the United States, several DSSs for commercial spent nuclear fuel are approaching the end of their initial licensed or certified term. Many of these systems were originally licensed or certified for 20 years, after which the licensing or certification may be renewed for periods up to 40 years, according to Title 10 of the *Code of Federal Regulations* (10 CFR), Part 72, "Licensing Requirements for the Independent Storage of Spent Nuclear Fuel, High-Level Radioactive Waste, and Reactor-Related Greater than Class C Waste." Guidance for review of renewal applications is provided in NUREG-1927 (NRC 2016), *Standard Review Plan for Renewal of Spent Fuel Dry Cask Storage System Licenses and Certificates of Compliance*. A review of aging effects that could affect important-to-safety structures, systems, and components is required in renewal applications and applicants are required to address aging effects using either a time-limited aging analysis or an aging management program. The U.S. Nuclear Regulatory Commission (NRC) issued NUREG-2214, *Managing Aging Processes In Storage (MAPS) Report* (NRC 2019), which provides guidance on the evaluation of known aging degradation mechanisms to determine if they could affect the ability of dry storage system components to fulfill their safety functions in the 20- to 60-year period of extended operation.

In the United States, the majority of DSSs can be referred to as welded canister systems. These systems typically consist of a stainless-steel shell into which the spent fuel is loaded prior to sealing by welding. The welded canisters are then placed into a concrete overpack that provides physical protection for the welded canister and serves to shield the radiation emanating from the spent fuel. More detailed descriptions of some vertical and horizontal welded canister DSS designs are included in Meyer et al. (2013). Concern regarding the potential degradation of welded canisters by CISCC was originally communicated by the NRC in a technical report (NRC 2014) and in NRC Information Notice 2012-20 (NRC 2012) titled, "Potential Chloride-Induced Stress Corrosion Cracking of Austenitic Stainless Steel and Maintenance of Dry Cask Storage System Canisters." Several instances of CISCC in exposed stainless-steel components at nuclear power plants (NPPs) in coastal environments are cited in Information Notice 2012-20. Although sheltered by the concrete overpack, welded canisters are still susceptible to exposure to chlorides and moisture that is carried by circulating air flow through ventilations in the overpack.

Periodic inspection of components with NDE is an integral part of aging management at NPPs. Metallic piping and vessel components are subject to visual, surface, or volumetric examinations depending on the mode of degradation and the important-to-safety function of the component. Inservice inspection requirements are included in Section XI of the American Society of Mechanical Engineers (ASME) Boiler and Pressure Vessel (B&PV) Code (ASME 2017). Common NDE methods used for NPP inspections include visual testing (VT), eddy current testing (ECT), and ultrasonic testing (UT). These methods are also applicable to the inspection of welded canisters in DSSs although there are challenges associated with accessibility of the canisters (Meyer et al. 2013). As a result, the industry, through the Electric Power Research Institute (EPRI), is developing robotic crawler technologies capable of carrying an NDE payload to the surface of a canister and facilitating remote examinations. EPRI has funded the development of robotic crawler systems for welded canisters and coordinated with utilities to conduct several demonstrations (EPRI 2016, 2017a). Efforts by some certificate of compliance (CoC) holders include the development of technologies for inspecting canisters outside of their overpacks. These technologies may incorporate multiple NDE technologies and obtain more complete access of canister surface areas (EPRI 2017b). An ASME B&PV Section XI Task Group titled "Inservice Inspection of

Spent Nuclear Fuel Storage and Transportation Containment Systems" has also been formed to develop requirements for the inspection of welded canisters in DSSs in draft Code Case N-860.

1.1 Purpose of this Report

The response of an NDE technology to a flaw depends on several factors related to the flaw size, shape, and morphology. In performance studies of NDE for dissimilar metal weld reactor components, a variety of techniques have been applied to simulate SCC flaws (Cumblidge et al. 2010; Meyer and Heasler 2017). Techniques include electro-discharge machining, coupon-implanted mechanical fatigue cracks, coupon-implanted thermal fatigue cracks (TFC), in situ grown TFCs, and weld solidification cracks. All the techniques are approximations of SCC flaws and the technique selection depends on several factors including the target application, practical constraints, and cost. The objective of this effort is to create actual SCCs in stainless-steel specimens so that the responses of NDE technologies can be evaluated using flaws with features (i.e., geometry and morphology) that are relevant to potential CISCC of stainless-steel canisters in DSSs for spent nuclear fuel.

The approach to producing desired specimens incorporated a "scoping" phase in which attempts at growing SCCs were performed using a smaller test rig and smaller test specimens. The scoping phase was necessary to explore test parameters and practical aspects of design through trial-and-error. After achieving satisfactory results in the scoping phase, the manufacture of the final NDE specimens in the full-scale test rig could begin with confidence. The approach for fabricating flaws in both the scoping phase and for production of final NDE specimens may be characterized as "cook-and-look." While such an approach may lack the precision and level of control offered by a highly instrumented test setup, the "cook-and-look" approach is adequate for creating NDE specimens.

The specimens that are the subject of this report consist of uniform base material. In the field, the concern with CISCC is focused on heat-affected-zones (HAZs) near welds. To avoid the additional complications of fabricating and testing specimens with welds, this effort focused on testing of base material. Following the identification of a successful procedure for fabricating flaws in base material, a potential next step is to fabricate flaws in welded specimens.

This report documents the approach to fabricating SCC specimens including a description of both the scoping phase and final test rig and test specimen designs in Section 2.0. Section 3.0 outlines the progression through the scoping phase by describing the results of the scoping tests, and Section 4.0 documents the NDE and destructive analysis performed on some of the specimens to characterize the flaws and confirm their size. Conclusions and suggestions for future work are included in Section 5.0.

2.0 Test Specimens and Test Rig Concepts

The test specimen designs and the test rig concepts used in this effort are described in this section. This includes descriptions of the specimens and test rig concept used during the scoping phase of testing and descriptions of the specimens and test rig concept for production of the final NDE specimens. As noted in the introduction, a scoping phase was employed using a smaller test rig and smaller specimens to facilitate adjustments to test parameters through trial-and-error.

2.1 Test Specimen Designs

Rectangular plate specimens of 304L stainless steel were selected to simulate a dry storage canister wall. The size of the plates was selected to ensure the final NDE specimens are large enough to accommodate instrumentation for ECT, bulk ultrasound testing, and guided-wave ultrasound testing. Guided-wave ultrasound testing techniques limit the minimum size of the specimens as they need to be large enough to ensure minimal edge effects and large enough to simulate the transducer-to-flaw distances anticipated for field applications (e.g., in some vertical systems, access to the canister surface is constrained in regions adjacent to channels on the overpack liner). Scoping phase specimens are not subject to the same size requirements and are made smaller to reduce consumption of material and to facilitate more convenient iteration of test parameters. Depictions of the geometries and dimensions for the final NDE specimens and for the scoping phase test specimens are provided in Figure 2-1. Photographs of the scoping phase specimens and final NDE specimens prior to application of masks are included in Figures 2-2 and 2-3, respectively. The plates for the final NDE specimens were ordered from plate stock already fabricated to the desired dimensions. For the scoping phase specimens, 4 × 24-inch plates were ordered and then cut down to 20 inches in length.

As Figure 2-1 illustrates, the specimens were designed with the intention of growing SCCs in the middle of the specimens. Although weld regions are considered the greatest risk for CISCC due to the presence of residual weld stress and sensitization of material in the HAZ, welds were not incorporated in these efforts to minimize the number of influencing parameters and provide a better chance of successful crack production.

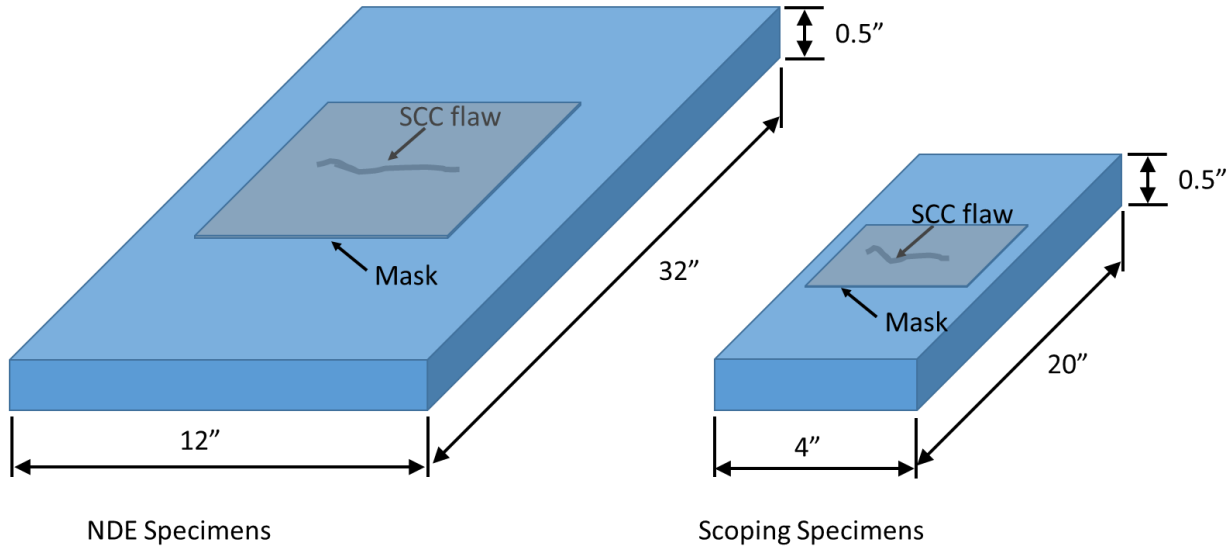

Figure 2-1. Depiction of plate geometry NDE specimens and scoping phase specimens.

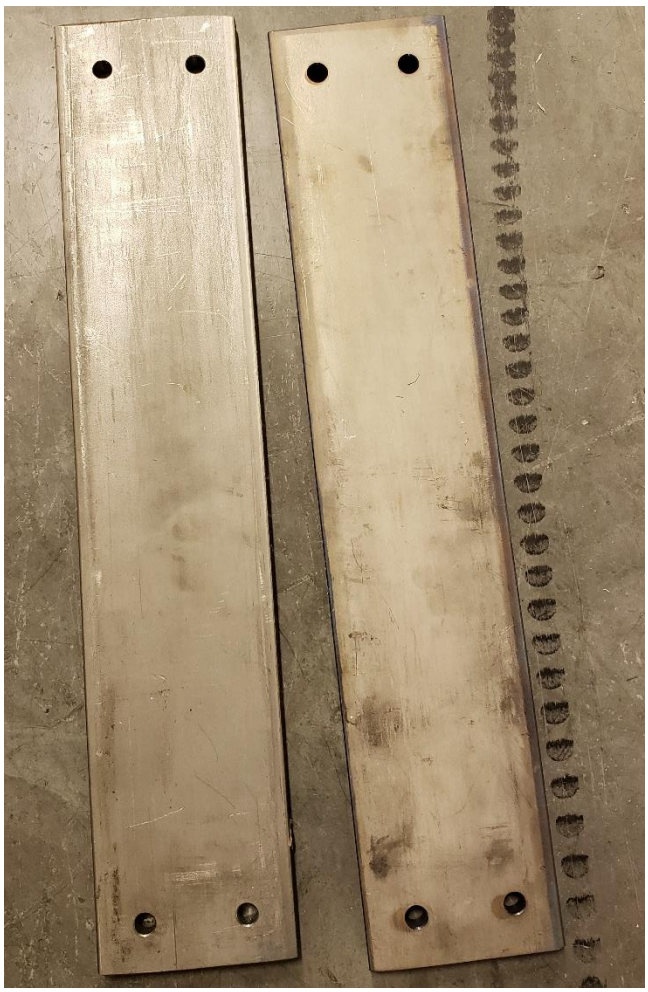

Figure 2-2. Photograph of scoping phase specimens prior to application of masks.

Most of the specimens were masked, as indicated in Figure 2-1, to control the location of SCC initiation without introducing a starter notch. Some of the initial scoping specimens were masked by applying a polyamide coating and using a Dremel tool to create a linear penetration of the coating in the region targeted for crack initiation. During later scoping phase iterations, a high-temperature engine enamel was applied as a mask. One line of tape was applied to the region of targeted crack initiation before applying the engine enamel. The tape was then removed before the enamel hardened to create the desired exposure pattern. The high-temperature engine enamel appeared to function more effectively than the polyamide coating for this purpose. The enamel mask could be removed from specimens for post-test analyses using acetone.

Sensitization of some specimens was performed to encourage SCC formation. In these cases, sensitization was performed by soaking the specimens in a furnace at 600°C for 40 hours. A photograph of the vacuum furnace used for sensitization of specimens is included in Figure 2-4.

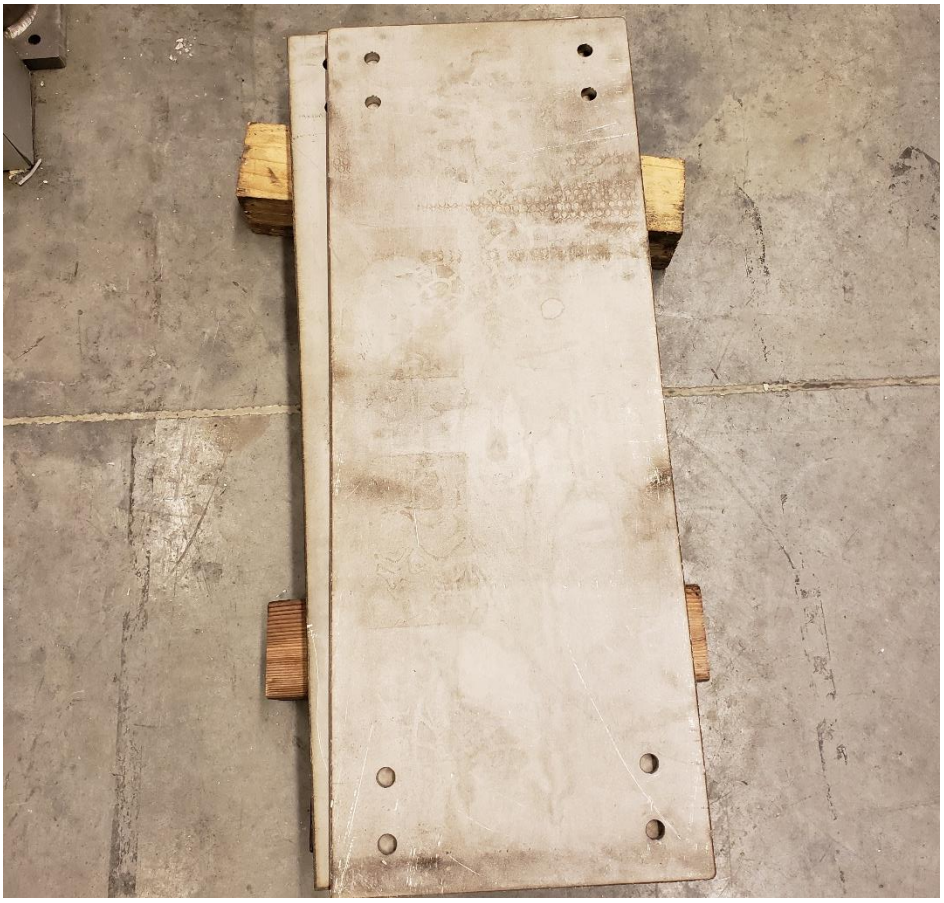

Figure 2-3. Photograph of final NDE specimens prior to application of masks.

Figure 2-4. Photograph of the vacuum furnace used for sensitizing specimens**.**

2.2 Test Rig Concepts

A test rig concept for growing CISCC flaws into plate specimens was developed that allowed the specimens to be stressed by a four-point bend loading mechanism and subject to a corrosive environment that was created through exposure to a high-temperature magnesium chloride hexahydrate solution ($MgCl_2 \bullet 6H_2O$). A photograph of the test rig for scoping phase testing is provided in Figure 2-5. Load is applied by tightening bolts that are installed in each end of the test specimens creating tensile stress on the bottom face of the test specimen in the region between the two inside contact points between the test specimen and cylindrical constraints (Figure 2-6).

Figure 2-5 shows that a cup containing $MgCl_2 \bullet 6H_2O$ is supported by a jack stand that can be manipulated to bring the cup containing $MgCl_2 \bullet 6H_2O$ in contact with the specimen surface. The $MgCl_2 \bullet 6H_2O$ solution is heated through the specimen using a copper heating element positioned above the specimen between the two inside constraint cylinders (Figure 2-6). The temperature of the $MgCl_2 \bullet 6H_2O$ solution is measured by a thermocouple inserted into the solution cup through the access port that can be seen in Figure 2-5.

Specimens were originally exposed from underneath, as depicted in Figure 2-5, to prevent leakage or spilling of the $MgCl_2 \bullet 6H_2O$ solution. However, to better ensure that the solution stayed in contact with the specimen, the test rig was reoriented onto its side so that the cup containing the $MgCl_2 \bullet 6H_2O$ solution contacted the specimen from the side instead of from underneath.

The cup containing the $MgCl_2 \bullet 6H_2O$ solution was initially made of polyvinyl chloride (PVC). However, the cup experienced some melting during testing of the first specimen and was replaced with one made of chlorinated polyvinyl chloride (CPVC).

A similar design was used for the test rig for manufacturing the final NDE specimens. This test rig is larger than the test rig for the scoping phase because of the larger test specimens. A photograph of the test rig is provided in Figure 2-7. The $MgCl_2 \bullet 6H_2O$ solution and the heating element are not displayed in this photograph. The illustration in Figure 2-8 notes the spacing of the four-point bend load constraints as well as the deflections of the scoping specimens and final NDE specimens when under load. Under these conditions, the maximum load on each individual constraint would be 4720 N (1061 lbs.) for the scoping specimens and 7549 N (1697 lbs.) for the NDE specimens for a nominal Modulus of Elasticity of 193 GPa (28,000 kips).

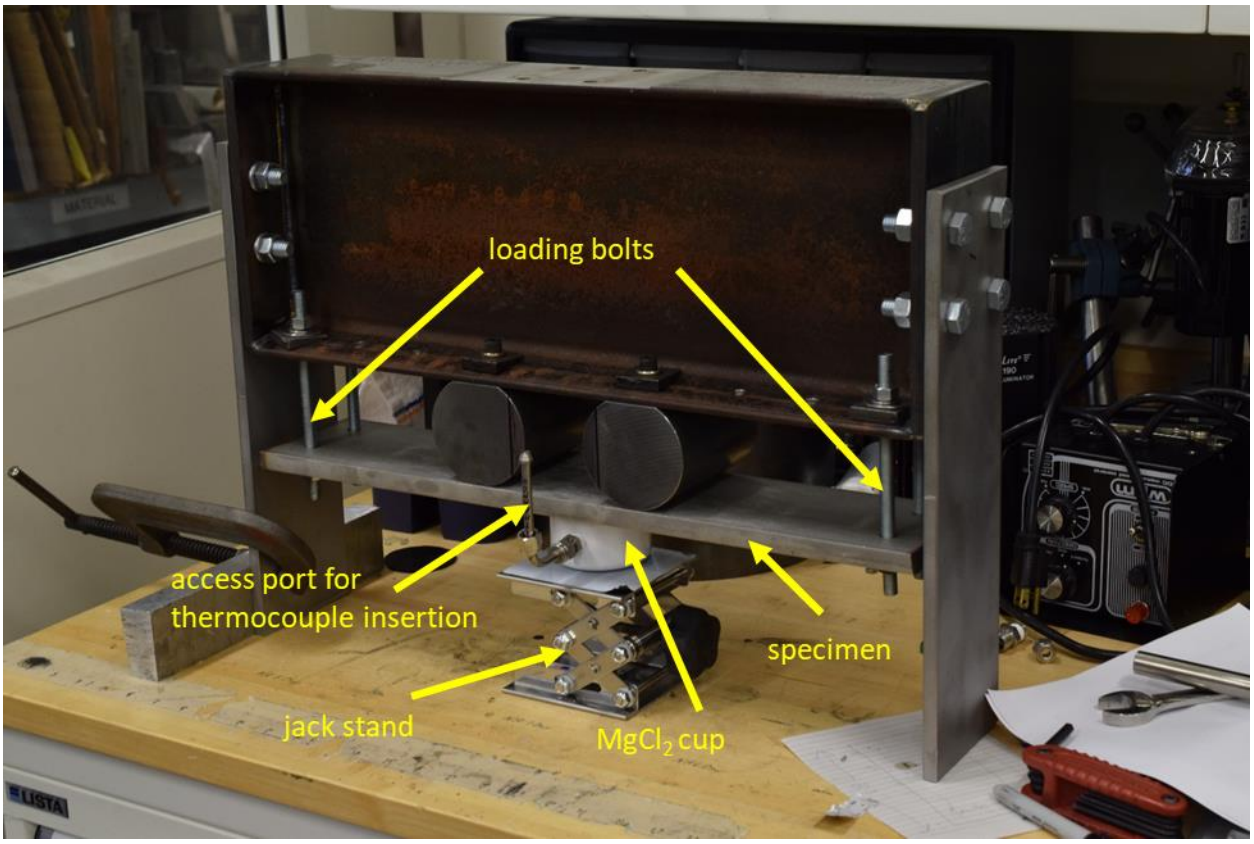

Figure 2-5. Photograph of test rig for scoping phase testing.

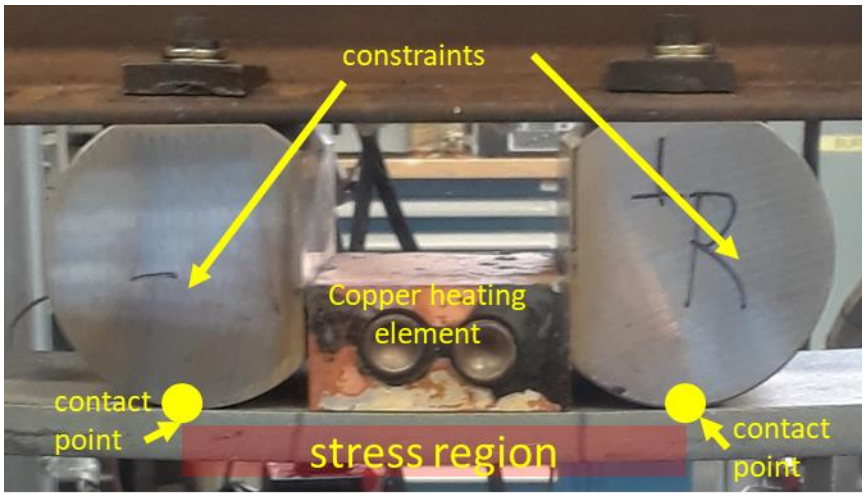

Figure 2-6. Photograph of copper heating element situated between the two inside contact points in the four-point bend loading configuration and on the side of the specimen opposite the $MgCl_2$ exposure and crack initiation.

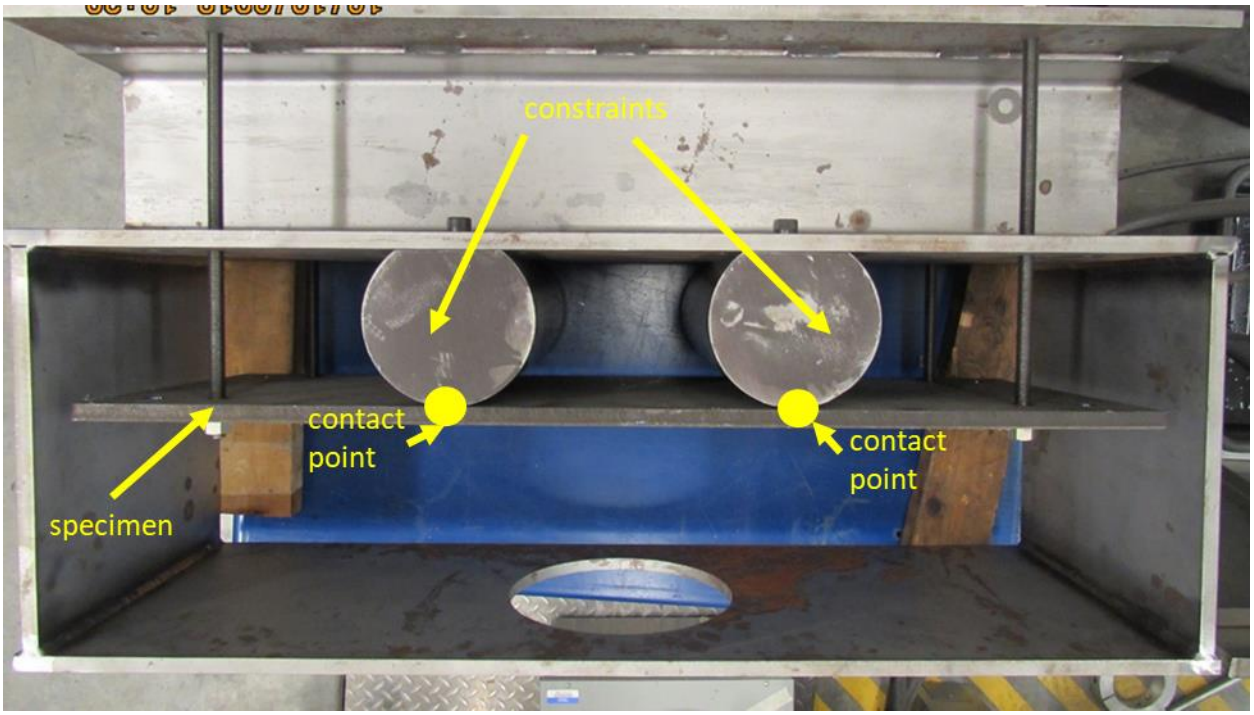

Figure 2-7. Photograph of larger test rig for manufacture of final NDE specimens.

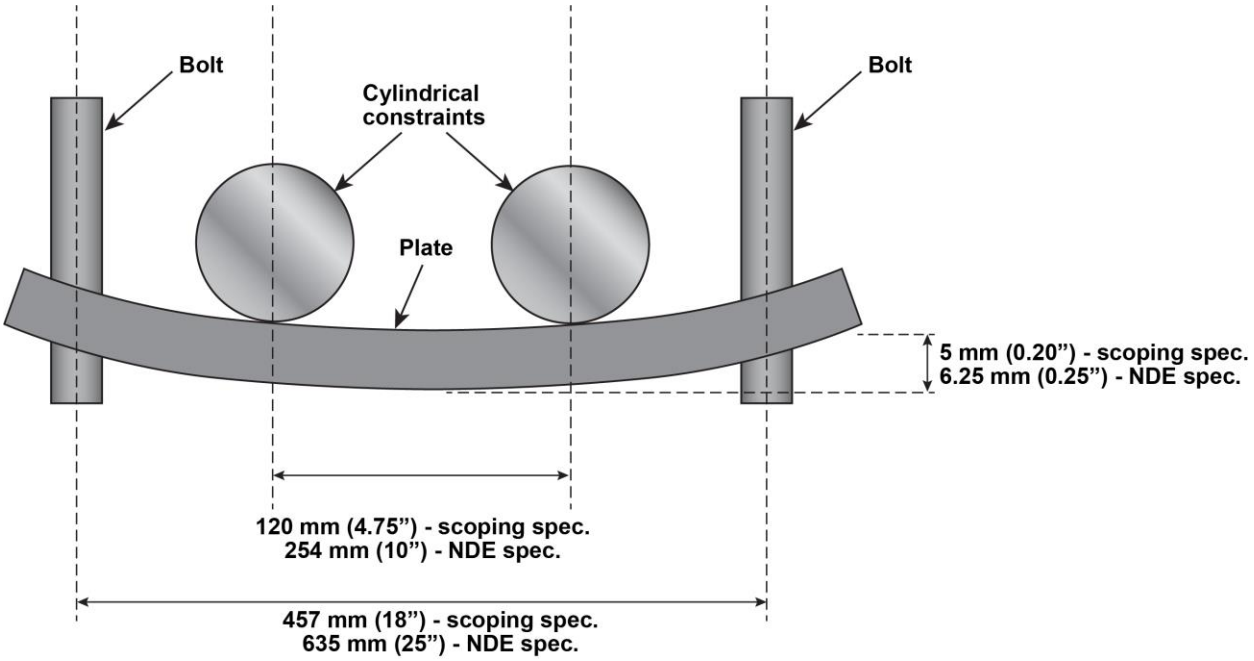

Figure 2-8. Illustration of four-point bend loading indicating dimensions of constraints and plate deflections under load.

3.0 Flaw Fabrication

This section discusses the trial-and-error testing conducted to refine a process to produce CISCCs for evaluating NDE technologies. This section provides an overview of the testing performed on seven scoping phase specimens and on one larger NDE specimen. Generally, the trial-and-error process involved adjustment of several test parameters including the $MgCl_2 \bullet 6H_2O$ solution concentration, the solution temperature, load applied to the specimens, and mask application. Photographs of most of the specimens post-test are provided. Further analysis was performed on some of the specimens to confirm the sizes of the cracks formed. The results of that analysis are included in Section 4.0.

3.1 Scoping Specimen 1

Scoping Specimen 1 was a scoping specimen that was unsensitized. A mask was created on the specimen by applying a polyamide coating and creating a linear penetration through the coating location by scratching with a razor blade. The specimen was exposed to $MgCl_2 \bullet 6H_2O$ using the test rig shown in Figure 2-5 and Figure 2-6 with the cup of $MgCl_2 \bullet 6H_2O$ oriented underneath of the specimen and raised up into contact with the specimen with the jack stand. The concentration of $MgCl_2 \bullet 6H_2O$ solution used for this test was in the range of 3–4 mol/L and the solution was heated to 100°C.

Testing of this specimen was terminated when it was discovered that the $MgCl_2 \bullet 6H_2O$ solution began to leak because the PVC cup holding the solution was melting. A photograph of the exposed area of the specimen after termination of the test is shown in Figure 3-1. The circular-shaped darkened region indicates where the $MgCl_2 \bullet 6H_2O$ solution was in contact with the specimen. The linear scratch in the polyamide mask is highlighted by the collection of precipitated $MgCl_2 \bullet 6H_2O$ crystals (white color). No crack formation was observed in this specimen.

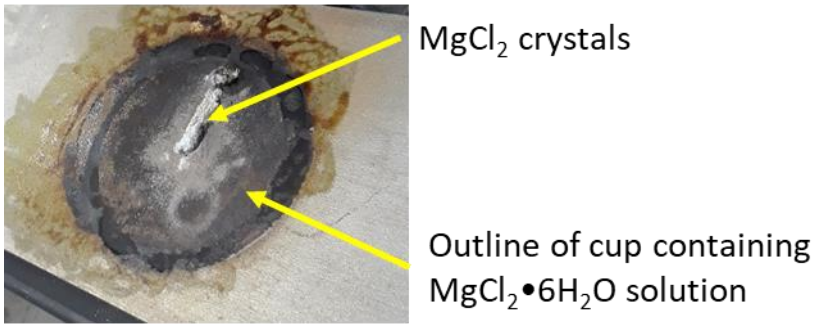

Figure 3-1. Photograph of Scoping Specimen 1 after removal from the test rig.

3.2 Scoping Specimen 2

A few adjustments were made in testing of Scoping Specimen 2. The PVC cup containing the $MgCl_2 \bullet 6H_2O$ solution was replaced with a cup fabricated from CPVC material. Also, Scoping Specimen 2 was sensitized by soaking the specimen in a furnace at 600°C for 40 hours. Finally, the concentration of the $MgCl_2 \bullet 6H_2O$ solution was strengthened to 6 mol/L. The solution was heated to 100°C. A polyamide mask was also applied to this specimen. However, a Dremel tool was used to create a linear penetration in the coating, instead of a razor blade. Scoping Specimen 2 was exposed to the $MgCl_2 \bullet 6H_2O$ solution for a week before terminating the test. A large crack was observed off to the side of the mask in a location

away from the mask penetration. A photograph of the plate after removal of the mask is shown in Figure 3-2. In this figure, the large crack and its location relative to the mask penetration can be observed.

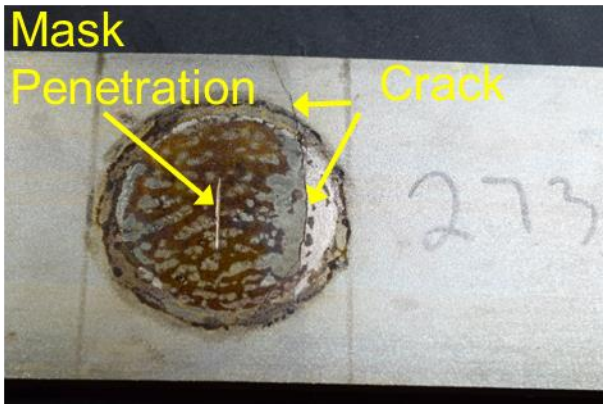

Figure 3-2. Photograph of Scoping Specimen 2 after termination of $MgCl_2 \cdot 6H_2O$ exposure and removal of polyamide mask.

3.3 Scoping Specimen 3

In preparation for Scoping Specimen 3, the test rig was modified so that the cup containing the $MgCl_2 \cdot 6H_2O$ solution contacted the face of the specimen from the side instead of from underneath. This adjustment was made to ensure that the $MgCl_2 \cdot 6H_2O$ solution was always in contact with the surface of the specimen, even if boiling occurred. Scoping Specimen 3 was sensitized by soaking the specimen in a furnace at 600°C for 40 hours. A polyamide coating was also applied to this specimen to provide a mask and a linear penetration in the mask was created using a Dremel tool. In an attempt to produce "tighter" cracks, the specimen was initially exposed to a milder $MgCl_2 \cdot 6H_2O$ solution (3 mol/L concentration) at 100°C. However, no cracks were yielded after two weeks of exposure, so the concentration was then increased to 6 mol/L and the solution was heated to 126°C. After making these adjustments, cracking was observed the following day. As with Scoping Specimen 2, the cracking was observed to the side of the masked region, away from the linear penetration, as can be seen in Figure 3-3.

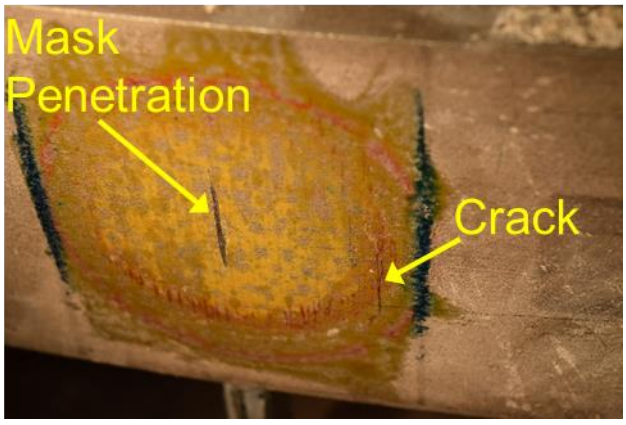

Figure 3-3. Photograph of Scoping Specimen 3 after termination of $MgCl_2 \cdot 6H_2O$ exposure and removal of polyamide mask.

3.4 Scoping Specimens 4 and 5

Scoping Specimens 4 and 5 were prepared without masks to observe how cracking would initiate in this scenario. These specimens were sensitized by soaking the specimen in a furnace at 600°C for 40 hours. They were both exposed to a saturated $MgCl_2 \cdot 6H_2O$ solution heated to 108°C. Many small cracks were observed in the specimens after exposure for two days. Photographs of the face of Scoping Specimen 5 are provided in Figure 3-4 and Figure 3-5. Without application of a mask barrier, there appears to be a tendency for specimens to shed stress by forming many shallow cracks in different locations instead of through formation of a few deep cracks.

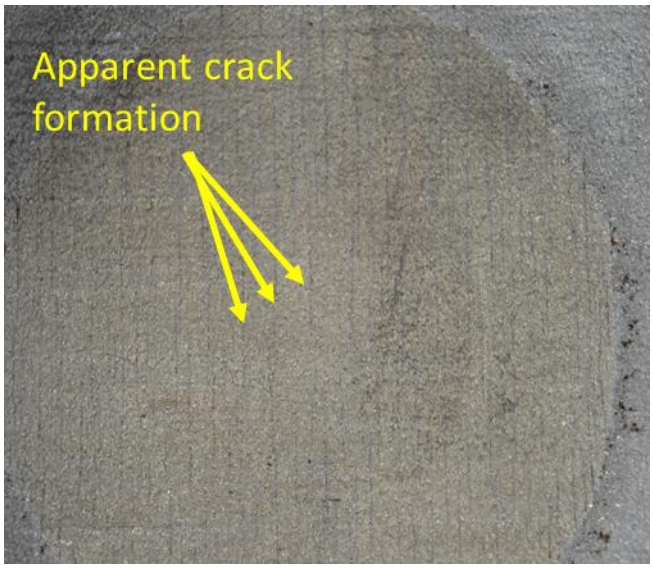

Figure 3-4. Photograph of Scoping Specimen 5 after termination of $MgCl_2 \cdot 6H_2O$ exposure.

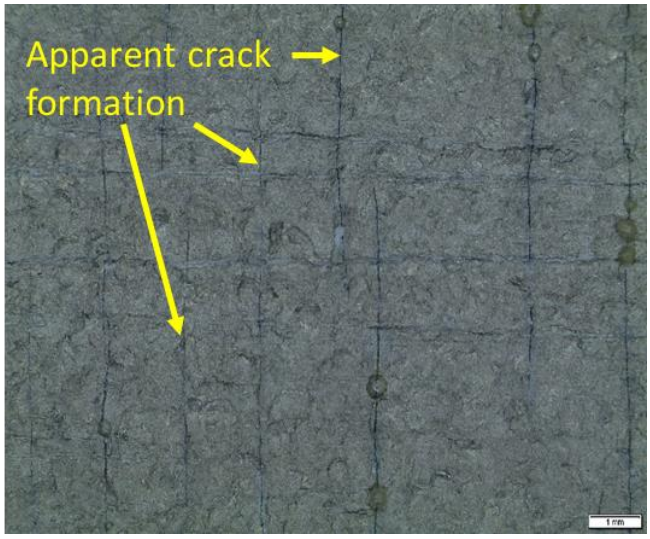

Figure 3-5. Close-up view of cracks formed in Scoping Specimen 5 after termination of $MgCl_2 \cdot 6H_2O$ exposure.

3.5 Scoping Specimens 6 and 7

Scoping Specimens 6 and 7 had a mask formed by coating a high-temperature enamel to the surface of the specimens. In Scoping Specimen 6, a linear region of exposure was created by scratching through the coating. In Scoping Specimen 7, a piece of thin tape was applied to the specimen before the application of the mask coating. The piece of tape was removed before solidification of the coating to create a linear exposed region. These specimens were sensitized by soaking the specimens in a furnace at 600°C for 40 hours. They were both exposed to a saturated $MgCl_2 \cdot 6H_2O$ solution heated to 108°C. They were both removed from the test rig after exposure for two days and crack formation was observed in each specimen. In these cases, the cracking was observed to occur in the target region exposed in the specimen mask.

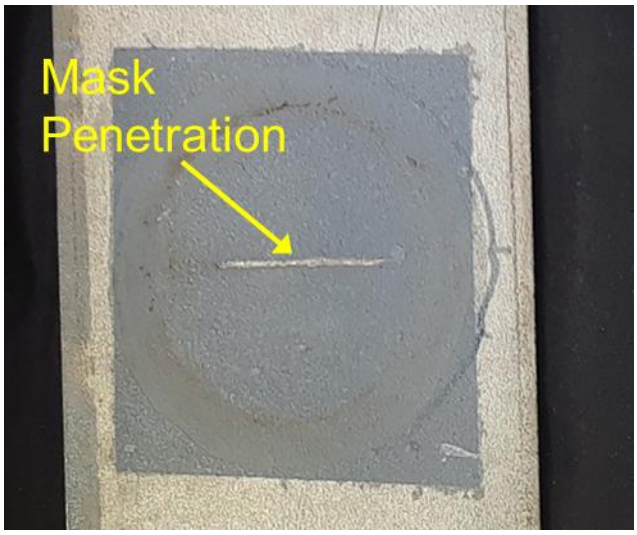

Figure 3-6. Photograph of high-temperature enamel mask applied to Scoping Specimen 6 with linear penetration created by scratch.

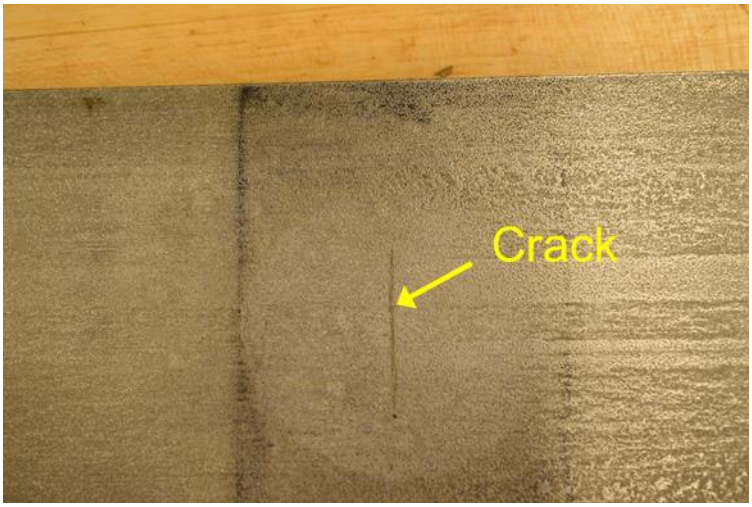

Figure 3-7. Photograph of Scoping Specimen 7 after removal of the high-temperature enamel mask to highlight crack formation in the targeted exposure region.

3.6 Scoping Specimen 8

A slight modification to the enamel mask was made for Scoping Specimen 8 to reduce the aspect ratio of the generated cracks. The length of the linear penetration in the mask was limited to ½ inches to target a 50% through-wall crack with 2:1 aspect ratio. Otherwise, this test was performed with the same parameters used for Scoping Specimens 6 and 7. A photograph of the high-temperature enamel mask and penetration on Scoping Specimen 8 prior to exposure to the $MgCl_2 \cdot 6H_2O$ solution is provided in Figure 3-8 and a photograph of the specimen after exposure and removal of the mask is provided in Figure 3-9.

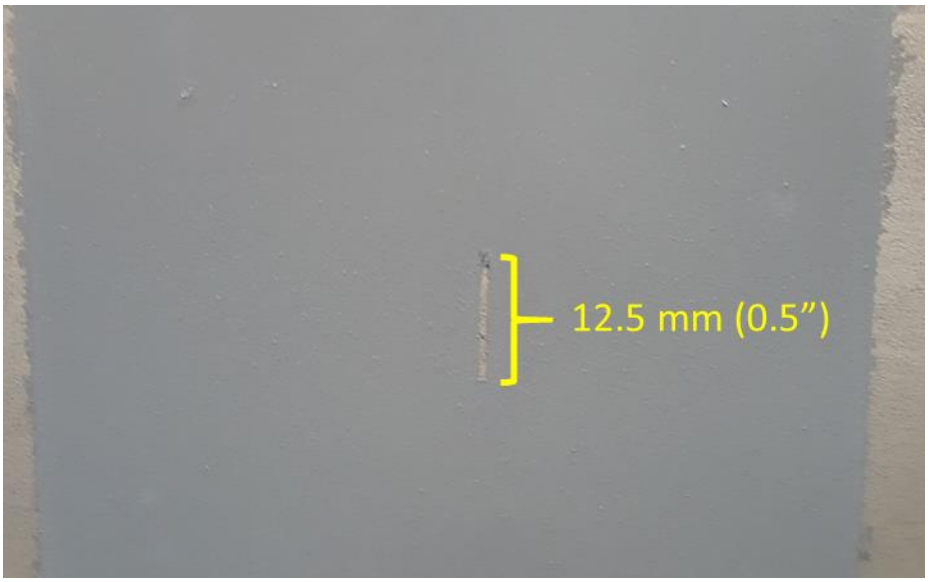

Figure 3-8. Photograph of high-temperature enamel mask applied to Scoping Specimen 8 before exposure to $MgCl_2 \cdot 6H_2O$ solution.

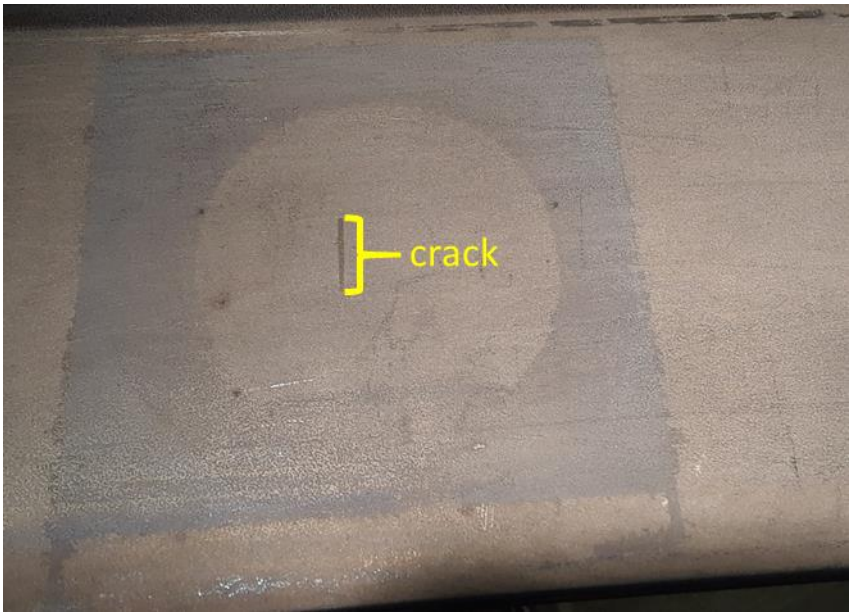

Figure 3-9. Photograph of Scoping Specimen 8 post-test and after removal of the high-temperature enamel mask.

3.7 NDE Specimen 1

The first large NDE specimen was manufactured following the testing of Scoping Specimen 8. The NDE specimen was fabricated by implementing best practices identified through the scoping phase. The specimen was initially sensitized by heating in a furnace at 600°C for 40 hours and a high-temperature enamel mask was applied to the specimen with a ½-inch long penetration to limit the aspect ratio of the flaw. The specimen was tested with a saturated $MgCl_2 \cdot 6H_2O$ solution heated to 108°C. Testing of the first NDE specimen proceeded cautiously and was removed from the test rig after 1 day of exposure to assess crack initiation and growth. A photograph of the specimen after exposure and removal of the mask is provided in Figure 3-10.

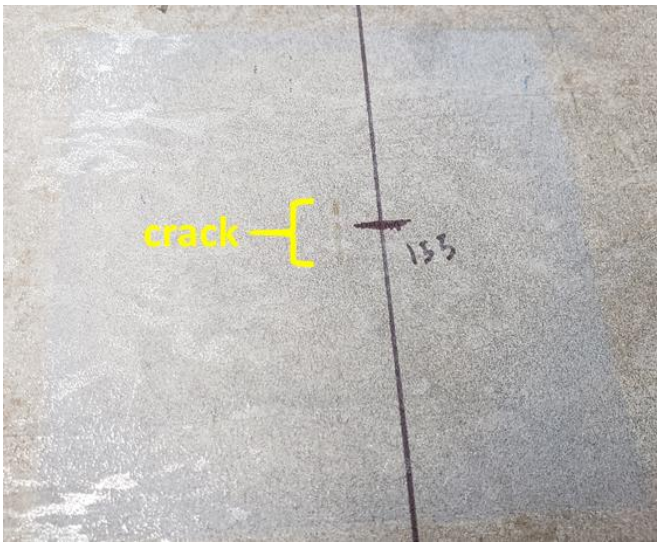

Figure 3-10. Photograph of NDE Specimen 1 post-test and after removal of the high-temperature enamel mask.

3.8 NDE Specimen 2

A second large NDE specimen was manufactured to grow a deeper crack in a large NDE specimen. The specimen was also initially sensitized by heating in a furnace at 600°C for 40 hours and a high-temperature enamel mask was applied to the specimen. The length of the penetration in this mask was not documented.

The specimen was tested with a saturated $MgCl_2 \cdot 6H_2O$ solution heated to 108°C. The specimen was initially exposed for 30 hours and then examined by manual UT and automated UT. Following these examinations, it was concluded that a crack may have initiated but no deep crack had formed yet. The specimen was exposed for another 24 hours to grow a deeper crack.

3.9 Summary

A summary of the testing conditions and test outcomes for the scoping specimen trials and the large NDE specimen, described in Sections 3.1–3.8, is provided in Table 3-1. The table also summarizes the result of NDE measurements performed on some of the specimens. A description of these measurements is provided in the next section (Section 4.0) and readers are encouraged to refer to Section 4.0 for more details regarding these measurements.

Table 3-1. Summary Table of Test Conditions and Test Outcomes for Scoping Specimen and Large NDE Specimen Fabrication

Specimen ID	Sensitized?	Concentration of $MgCl_2•6H_2O$	Temp.	Mask Technique	Outcome/Comments
1	No	3–4 mol/L	100°C	• polyamide coating with scratch by razor blade to penetrate coating	• No cracking observed • Testing terminated when PVC cup holding $MgCl_2•6H_2O$ solution melted
2	Yes	6 mol/L	100°C	• polyamide coating applied and Dremel used to penetrate coating	• Cup replaced with a CPVC cup for holding $MgCl_2•6H_2O$ solution • 1 week of exposure • Large crack occurred off to side in location away from coating penetration
3	Yes	3 mol/L for two weeks; 6 mol/L for 1–2 days	100°C for two weeks; 126°C for 1–2 days	• polyamide coating applied and Dremel used to penetrate coating	• Apparatus was modified so that solution was in contact with the specimen from the side instead of from underneath • Initial run for 2 weeks at 3 mol concentration—no cracking; increased solution to 6 mol concentration and got cracking overnight • Cracking is off to the side, away from the location of the coating penetration • Crack appears to be ~50% TW based on automated UT measurements • Estimated aspect ratio = 6.3:1 to 7.3:1
4 & 5	Yes	Saturation Concentration	108°C	• no masking	• Exposed for 2 days • Observed initiation of many shallow cracks in the specimen • Attempts to depth size cracks in Specimen 4 with UT were unsuccessful • Cracks likely < 2–3 mm in depth
6	Yes	Saturation Concentration	108°C	• high-temperature enamel coating applied with scratch by razor blade to penetrate coating	• Exposed for 2 days • Cracking was observed to occur where mask coating was penetrated

Specimen ID	Sensitized?	Concentration of $MgCl_2 \cdot 6H_2O$	Temp.	Mask Technique	Outcome/Comments
7	Yes	Saturation Concentration	108°C	• high-temperature enamel coating applied • strip of tape applied before application of coating and then removed to create penetration	• Exposed for 2 days • Cracking was observed to occur where mask coating was penetrated • Crack appears to be ~39% TW based on automated UT measurements • Estimated aspect ratio = 7.7:1 to 9.2:1
8	Yes	Saturation Concentration	108°C	• penetration in high-temperature enamel mask shortened to 0.5 in." • strip of tape applied before application of coating and then removed to create penetration	• Exposed for 2 days • Cracking was observed to occur where mask coating was penetrated • Crack appears to be ~73% TW based on manual UT measurements • Estimated aspect ratio = 3.1:1
Large Specimen 1	Yes	Saturation Concentration	108°C	• penetration in high-temperature enamel mask shortened to 0.5 in. • strip of tape applied before application of coating and then removed to create penetration	• Exposed for 1 day • Cracking was observed to occur where mask coating was penetrated • Attempts to depth size crack were unsuccessful • Crack is likely < 2–3 mm in depth
Large Specimen 2	Yes	Saturation Concentration	108°C	• penetration in high-temperature enamel mask • strip of tape applied before application of coating and then removed	• 1st exposure for 30 hours and 2nd exposure for 24 hours • Plate was UT scanned at multiple angles: 45°, 60°, and 70° • Crack appears to be ~64% TW based on automated UT measurements • Estimated aspect ratio = 5.25:1

4.0 Characterization of Specimen Flaws

Cracks created in specimens were examined nondestructively using UT, ECT, and VT technologies. UT was performed using a conventional single-element probe with shear-wave mode excitation and with a 5 MHz resonance frequency at a 45° angle. UT data could be acquired in both automated and manual methods. A mechanized scanner was set up to collect data from specimens with a 0.5 × 1.0 mm (scan × index) raster scan. A photograph of the automated setup applied to Scoping Specimen 3 is provided in Figure 4-1. The photograph shows the scanning track and X-Y manipulator along with a water catch basin, hose for application of water couplant, and the specimen. Automated scanning can be performed for either side of the specimens using half-V or full-V sound paths. Half-V examinations were performed from the side opposite from the crack opening; full-V examinations were performed from the crack opening surface. Depictions of the half-V and full-V sound paths are provided in Figure 4-2.

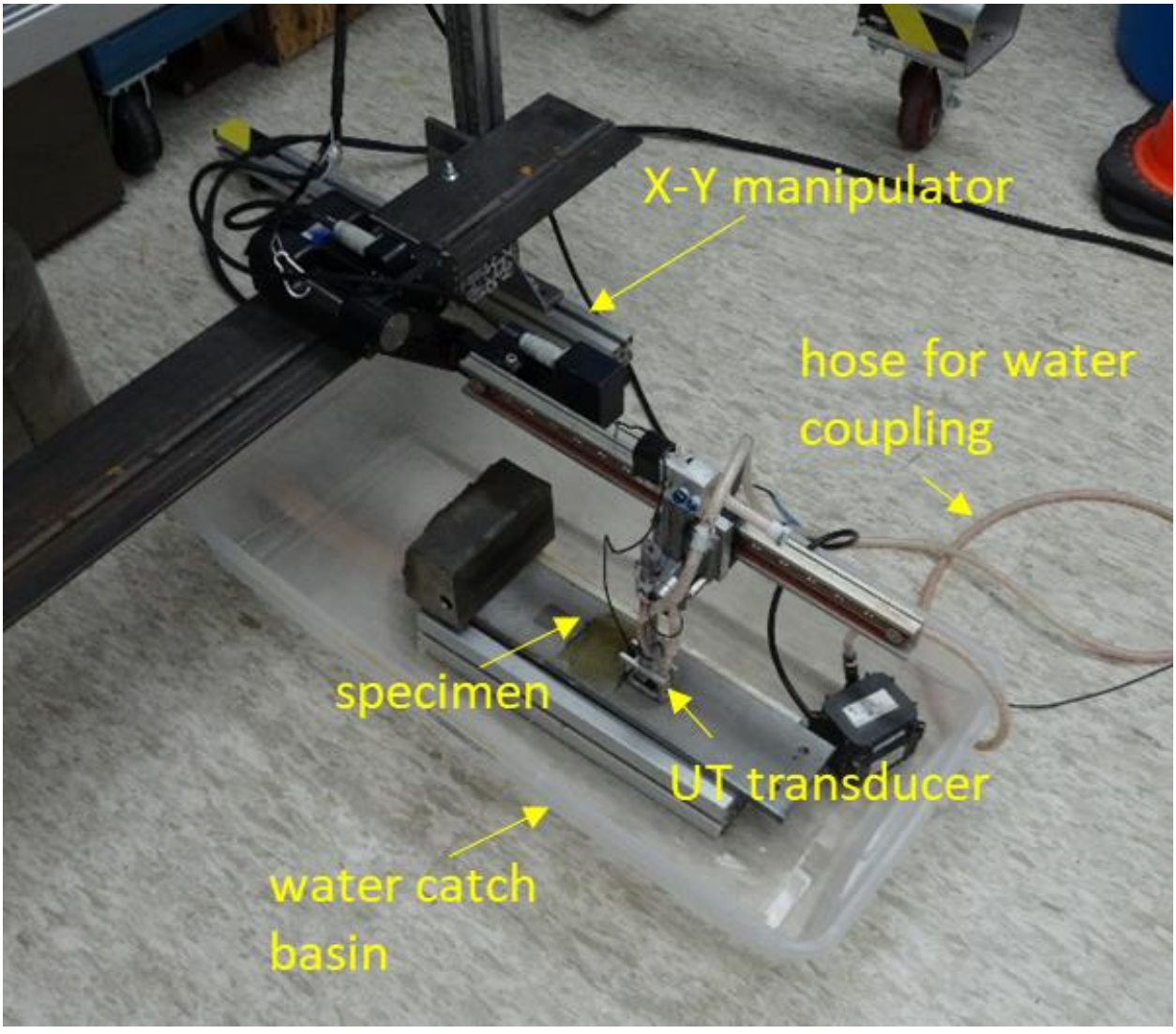

Figure 4-1. Photograph of automated UT scanning setup applied to Scoping Specimen 3.

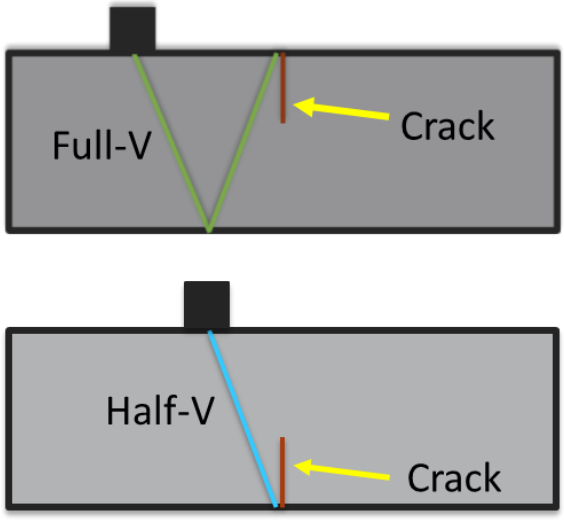

Figure 4-2. Depiction of full-V and half-V examinations of cracks.

A manual UT examination system was also used for performing examinations while specimens were mounted in the test rig. This system was set up with the same 5 MHz shear-wave probe at a 45° angle. A General Electric model USN60 pulser-receiver was used to excite and receive the signals. A photograph of the manual UT setup applied to Scoping Specimen 3 is shown in Figure 4-3. Petroleum jelly is used to couple the UT probe to the specimen for the manual examinations. Manual UT was used in addition to automated UT because of the convenience with performing the measurements without removing specimens from the test rig. The manual UT measurements enabled measurements of crack depth while the specimens were subjected to load. This could potentially result in more accurate measurements of crack depth than could be obtained by automated UT if crack closure upon removal of load caused underestimation of crack depth.

Detection of cracks by UT is based on the "corner" response, which is the coherent scattering of the UT signal by interaction of the incident energy with the intersection of the crack face and specimen surface, as depicted in Figure 4-4. Depth sizing of cracks by UT is based on the detection of a crack tip diffraction signal and the corner response signal as depicted in Figure 4-5. The depth of the crack can be obtained from the time difference in arrival of the crack tip signal and the corner response signal. Crack tip response signals are generally much weaker than corner response signals, making depth sizing of cracks more challenging than simply detecting cracks. Further, because depth sizing is based on the time separation of the crack tip response signal and corner response signal, depth sizing is not possible if cracks are so shallow that the crack tip response is overwhelmed by the corner response. For this purpose, it is estimated that cracks shallower than approximately 2–3 mm cannot be depth sized.

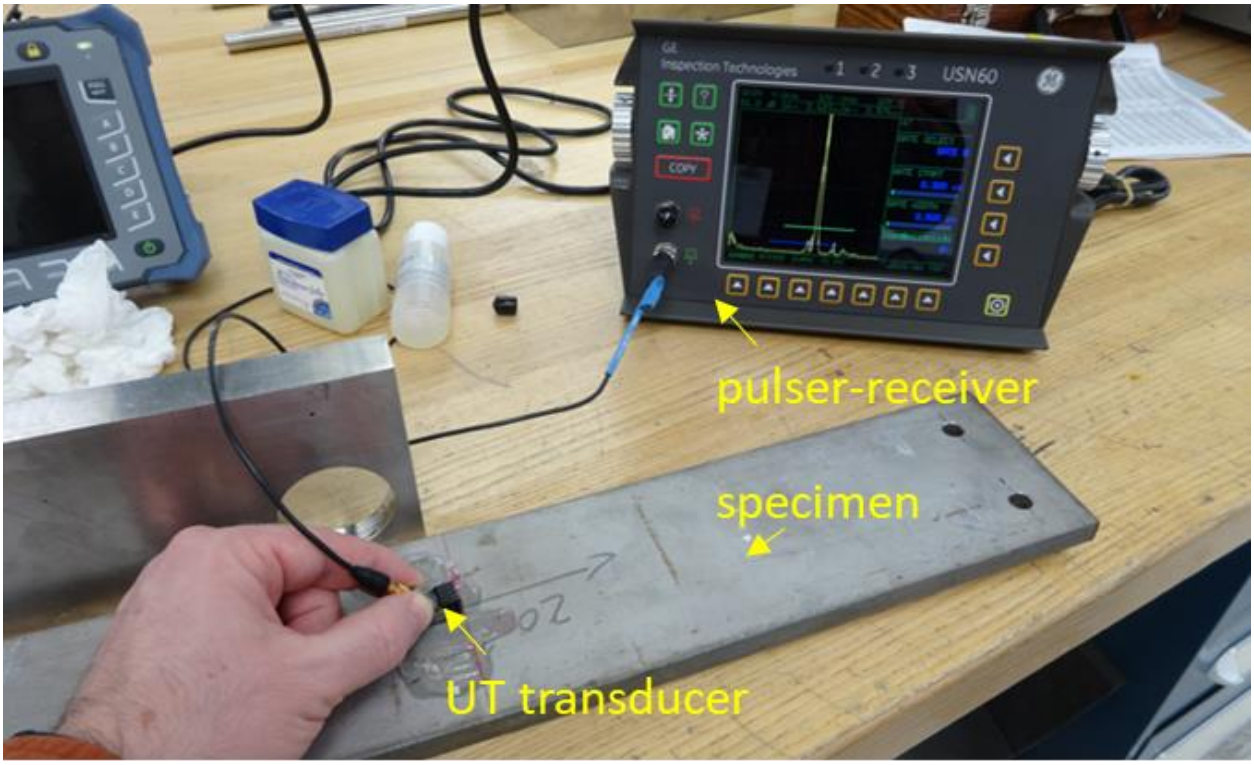

Figure 4-3. Photograph of the manual UT setup applied to Scoping Specimen 3 with A-scan response shown on the USN60 display.

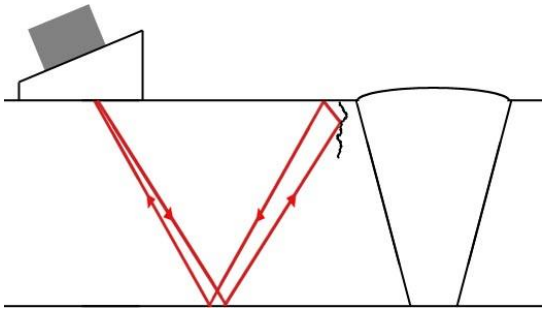

Figure 4-4. Depiction of coherent scattering of a UT signal from the corner formed by the intersection of a crack face with a specimen surface.

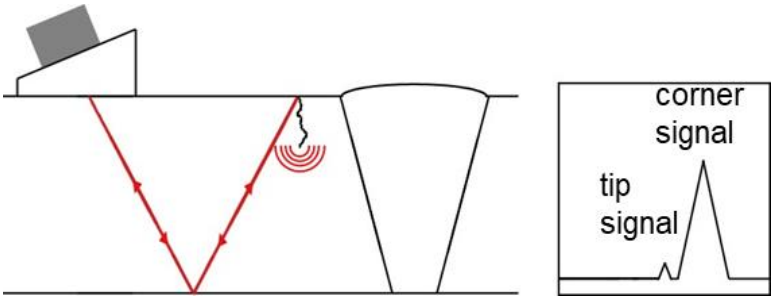

Figure 4-5. Depiction of a crack tip diffraction signal and a corner response signal in a UT response.

ECT data was acquired with a WesDyne data acquisition system and automated scanner. Data was collected at multiple frequencies ranging from 0.2 MHz up to 2.0 MHz with a Uniwest absolute probe. ECT was performed after removal of the enamel mask with acetone. Photographs of the automated scanner setup and the ECT probe scanning over the surface of Scoping Specimen 7 are provided in Figure 4-6 and Figure 4-7.

Finally, an optical profilometer was employed to characterize the crack opening displacement (COD) of the crack fabricated in Scoping Specimen 7. A photograph of the optical profilometer is included in Figure 4-8.

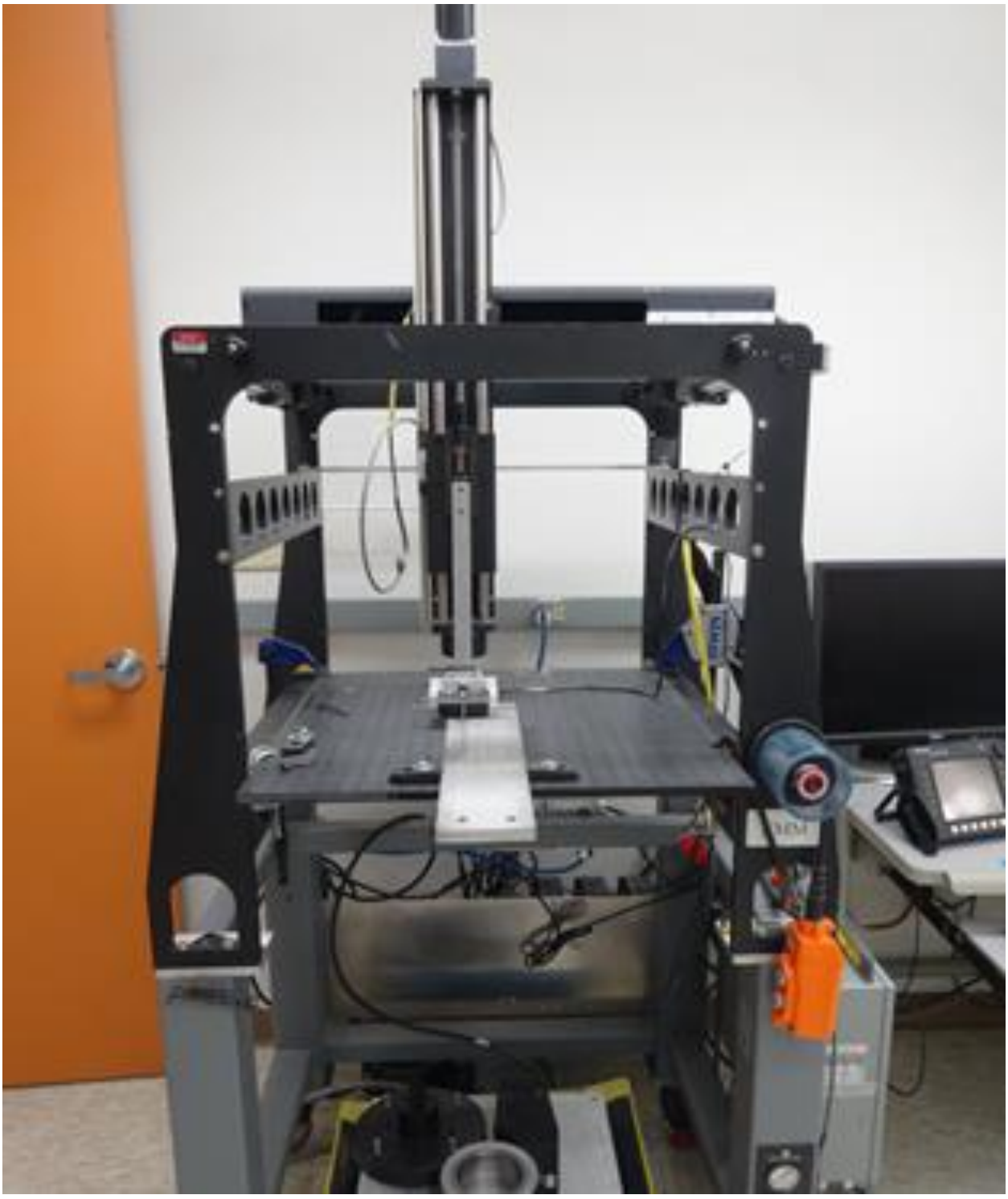

Figure 4-6. Photograph of the automated scanning system and X-Y-Z manipulator for ECT examinations.

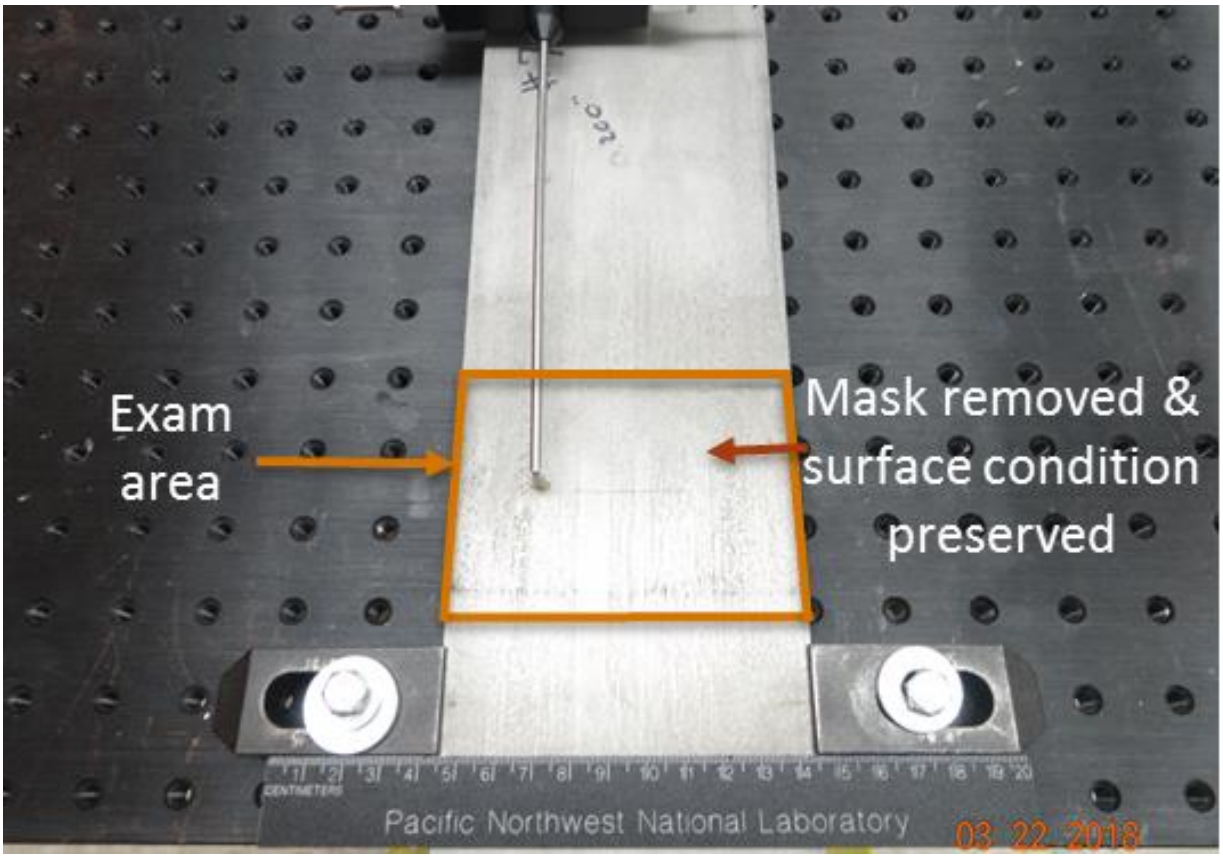

Figure 4-7. Photograph of absolute probe scanning over the surface of Scoping Specimen 7.

Figure 4-8. Photograph of optical profilometer.

4.1 Characterization of Scoping Specimen 3

The crack generated in Scoping Specimen 3 was characterized nondestructively using the automated UT method described above. Characterization by ECT was not considered useful, in this case, because the flaw was large with a significant and visually obvious crack opening. The flaw was also destructively analyzed to characterize the nature of the cracks as propagating transgranularly or intergranularly. The full-V response for Scoping Specimen 3 is provided in the series of response images in Figure 4-9. In the C-scan response image (viewing into the specimen from above–*top right*), an approximate outline of the area exposed to $MgCl_2 \cdot 6H_2O$ can be observed. The response from the large crack generated because of $MgCl_2 \cdot 6H_2O$ exposure is annotated and located to the side of the region, away from where the mask was penetrated, consistent with Figure 3-3. In addition to a response from the large crack, there appear to be several other smaller indications signifying the initiation of additional cracks that were not visible. The corner response from the flaw is depicted in the D-scan response (viewing into the specimen from end–*bottom left*). This image also depicts a response from the crack tip, which does not appear to persist over the full length of the crack. From this image response, an estimation of the crack length and depth can be obtained. The length of the crack can be estimated from the corner response, which is labeled as "Crack Side Profile" based on the distance between 6 dB drop-off locations on each end of the crack. The length of the crack is estimated to be 42 mm (1.65 in.) and the depth of the crack is estimated to be 6.7 mm (0.264 in.) [52.8% through-wall].

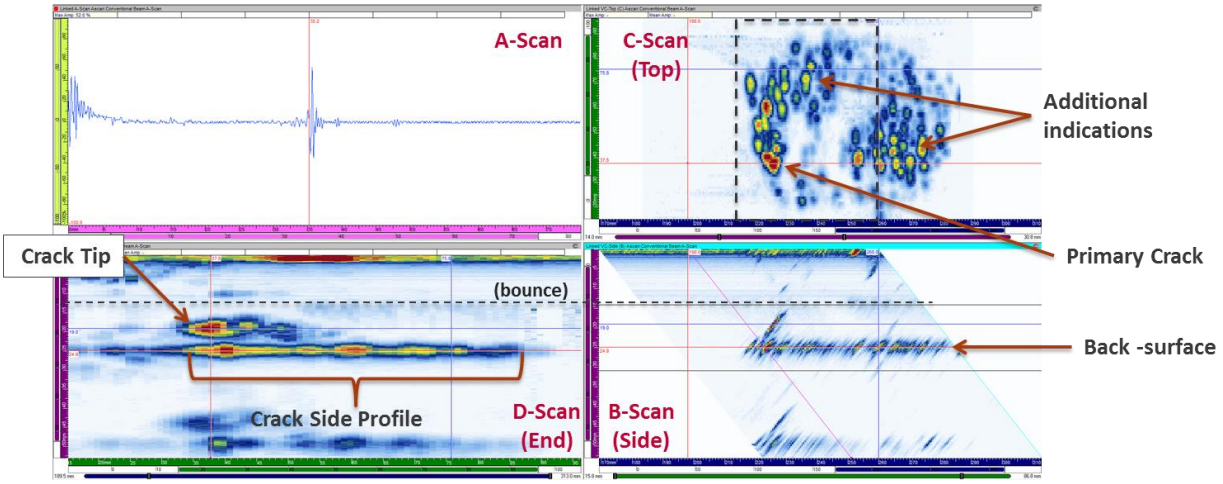

Figure 4-9. Response images obtained from a full-V automated UT examination of Scoping Specimen 3 (*top left*: A-scan, *top right*: C-scan, *bottom left*: D-scan, *bottom right*: B-scan).

The half-V response obtained from automated UT examination is provided in Figure 4-10. Overall, the response images appear very similar to those for the full-V examination in Figure 4-9. A slightly different estimate of flaw depth is obtained from these response images: 5.76 mm (0.227 in.) [46% through-wall].

Manual UT was also performed on Scoping Specimen 3 by the half-V examination method. A recorded response is not generated by manual UT, but the measurement of depth was consistent with the depth measurement obtained by the half-V automated UT examination. In this case, a depth measurement of 5.8 mm (0.228 in.) [46% through-wall] was obtained.

A summary of crack size estimations for the crack in Scoping Specimen 3 is provided in Table 4-1. The aspect ratio obtained from these estimates ranges from 6.3:1 to 7.3:1.

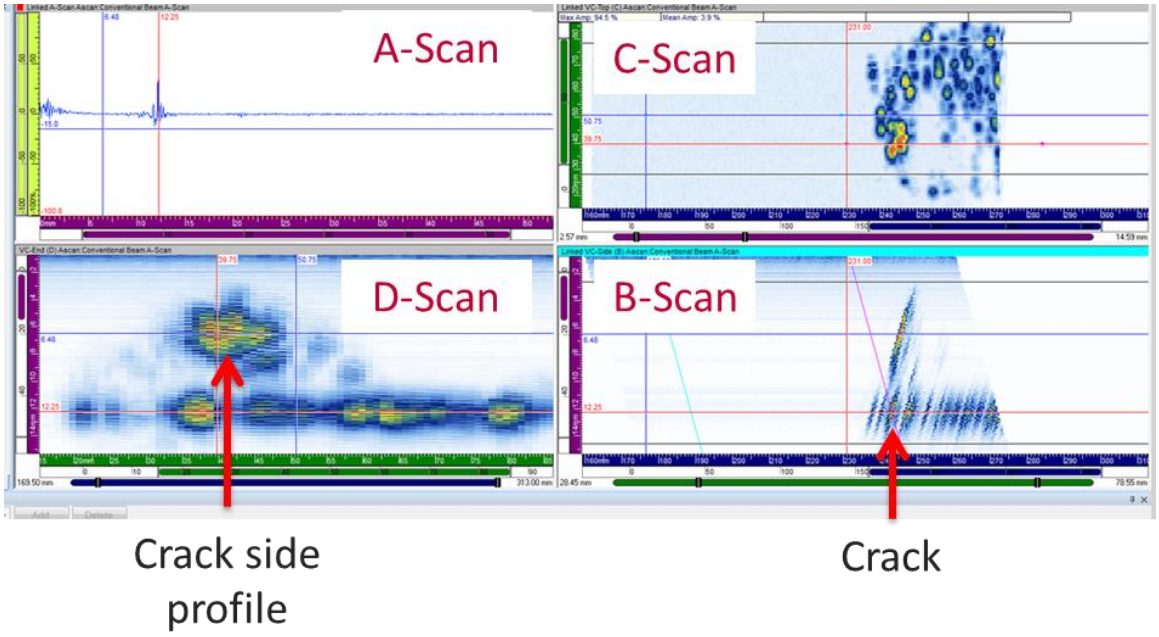

Figure 4-10. Response images obtained from a half-V automated UT examination of Scoping Specimen 3 (*top left*: A-scan, *top right*: C-scan, *bottom left*: D-scan, *bottom right*: B-scan).

Table 4-1. Summary of Scoping Specimen 3 crack size estimations obtained from UT measurements and Destructive Analysis.

	Depth Estimate	Length Estimate
Automated full-V	53% through-wall 6.6 mm (0.26 in.)	42 mm (1.65 in.)
Automated half-V	46% through-wall 5.8 mm (0.23 in.)	---
Manual half-V	46% through-wall 5.8 mm (0.23 in.)	---
Destructive Analysis	67% to 75% through-wall	
Estimated aspect ratio – 6.3:1 to 7.3:1		

Destructive analysis was performed on the crack in Scoping Specimen 3 by slicing the specimen into cross-sectional samples and polishing and etching the surfaces. A typical cross-sectional image (unetched) of the crack in Scoping Specimen 3 is shown in Figure 4-11. A scale is provided in the top right of the image, which can be used to estimate the dimensions of the crack. A review of the image indicates that UT examination underestimated the crack depth. In this image, the depth of the crack is between ⅔ (67%) and ¾ (75%) of the specimen thickness.

Higher magnification images of etched samples are provided in Figure 4-12 and Figure 4-13 with scales provided in the lower right corners of the images. The primary crack is easily visible in Figure 4-12 along with what appear to be smaller secondary cracks. The COD of the primary crack is approximately 150 µm. The CODs of the secondary cracks appear to be closer to 10 µm. These images indicate transgranular crack propagation for the primary crack and some of the secondary cracks. It also appears that intergranular mode crack propagation occurs as the main cracks branch off into smaller cracks.

Figure 4-11.Cross-sectional image (unetched) of crack in Scoping Specimen 3.

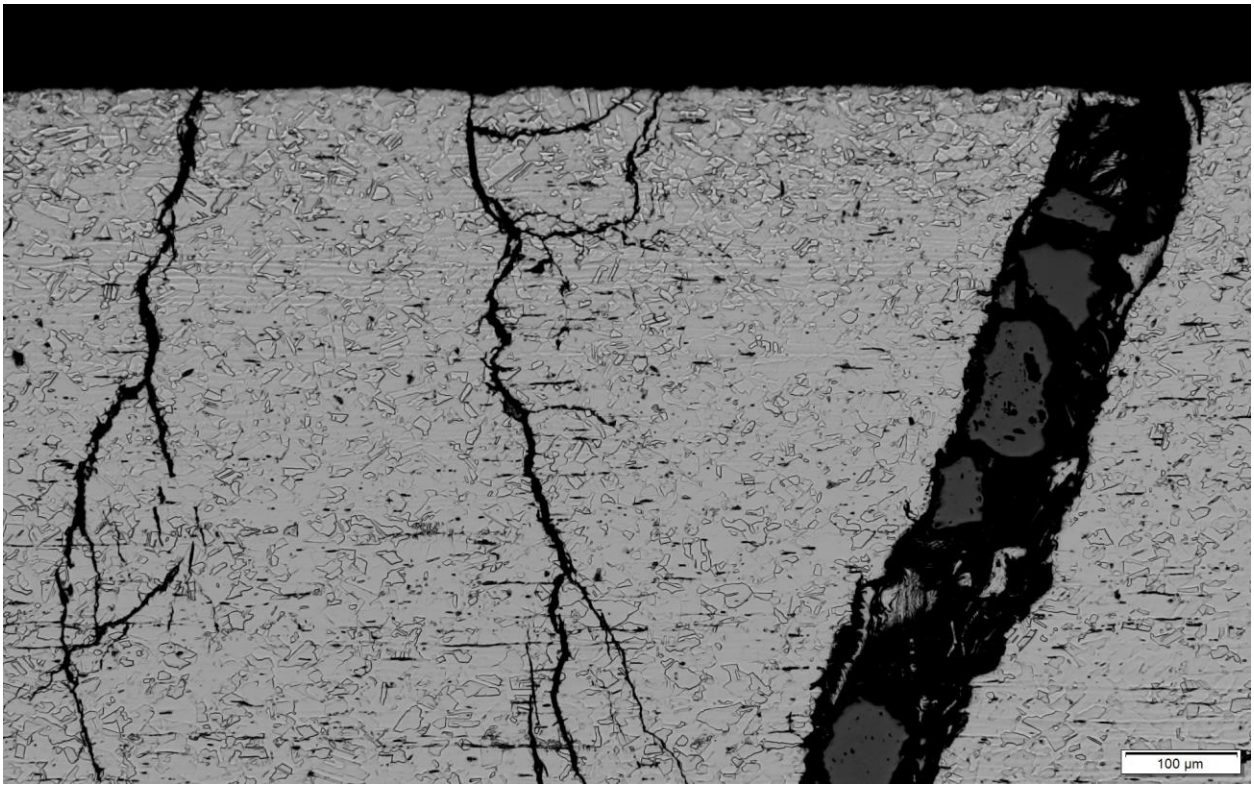

Figure 4-12. Cross-sectional image (etched) of crack in Scoping Specimen 3 near the surface.

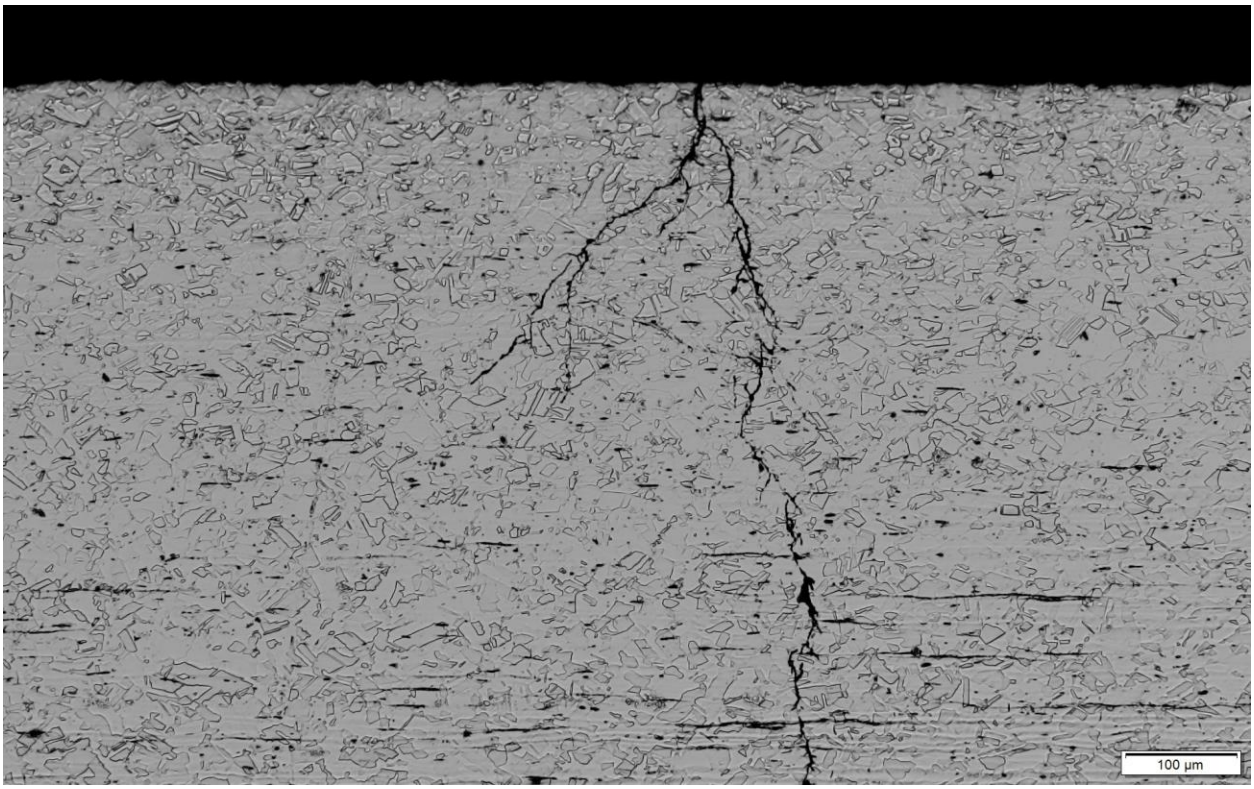

Figure 4-13. Cross-sectional image (etched) of a secondary crack in Scoping Specimen 3 near the surface.

4.2 Characterization of Scoping Specimen 4

As described in Section 3.4, Scoping Specimens 4 and 5 were tested without a mask to observe how cracking may initiate without masking the specimen surface. Visual examination of the specimens after testing appeared to reveal the formation of many small cracks. UT characterization of Scoping Specimen 4 was carried out to determine the significance of the cracks formed (i.e., if any deep cracks had formed). An automated half-V examination was performed, and the response images obtained are included in Figure 4-14. The C-scan response (*top left*) shows many small indications that could represent cracks initiating in the region exposed to the $MgCl_2 \cdot 6H_2O$ solution. However, no visible tip response is observed in any of the response images. This indicates that any cracks that have formed are too shallow for depth sizing (depth < 2-3 mm).

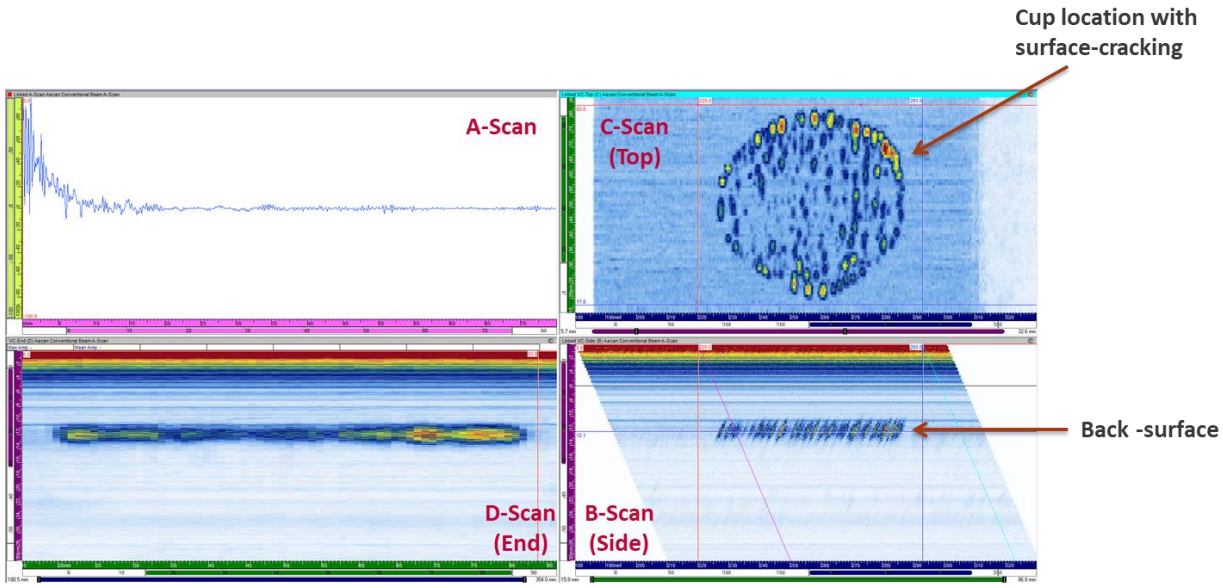

Figure 4-14. Response images obtained from a half-V automated UT examination of Scoping Specimen 4 *(top left*: A-scan, *top right*: C-scan, *bottom left*: D-scan, *bottom right*: B-scan).

4.3 Characterization of Scoping Specimen 7

Scoping Specimens 6 and 7 were prepared with a high-temperature enamel mask. UT and ECT examinations were performed on Scoping Specimen 7 to confirm conclusions drawn from visual examination of the specimen post-test. An automated half-V examination was conducted, and the response images obtained are included in Figure 4-15. The C-scan (*top left*) response images displayed a strong response in the region the mask was penetrated, confirming that the high-temperature mask was successful in isolating primary crack growth to the desired location. The C-scan image also shows some secondary indications, likely caused by the initiation of smaller cracks. A crack tip response could also be identified in the D-scan image (*bottom right*). Although the crack tip response does not appear to be as strong as the tip response observed for Scoping Specimen 3 in Figure 4-9; in this case, the tip response does appear to persist over most of the length of the crack.

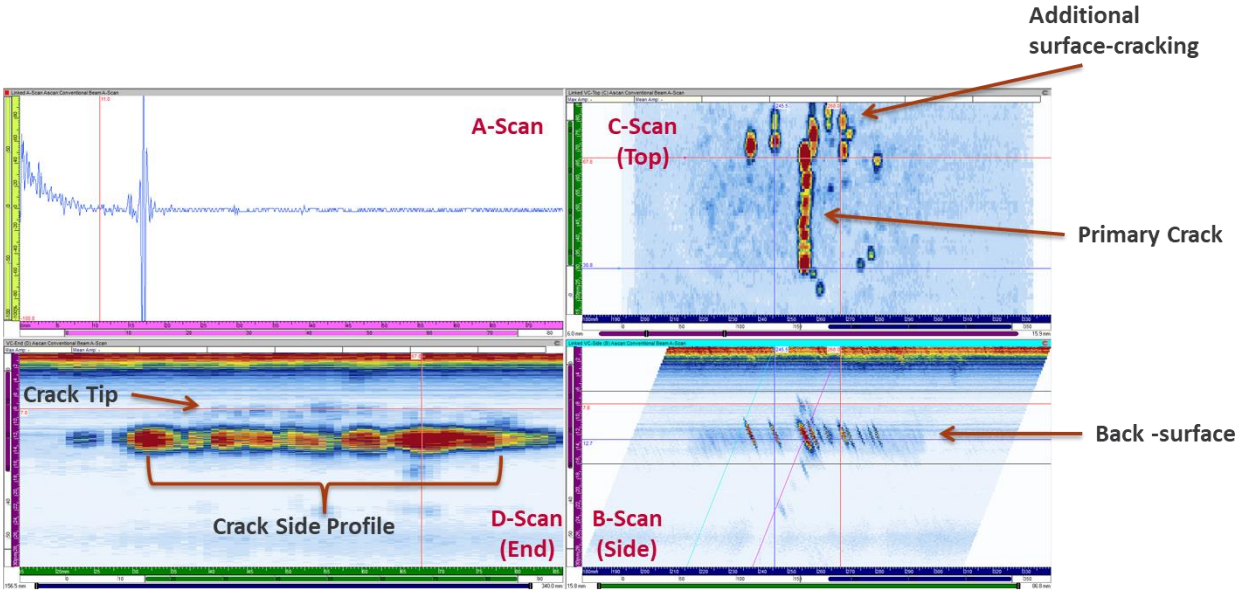

Figure 4-15. Response images obtained from a half-V automated UT examination of Scoping Specimen 7 (*top left*: A-scan, *top right*: C-scan, *bottom left*: D-scan, *bottom right*: B-scan).

ECT examination was also performed on Scoping Specimen 7, and the resulting response image for the ECT scan at 750 kHz is provided in Figure 4-16. The ECT examination helped confirm the nature of the secondary indications in Scoping specimen 7. Because many of the secondary indications also appear in the ECT response images, the data confirms these indications are surface-breaking and likely represent the initiation of additional cracks. The ECT examination also facilitated a more accurate estimate of the crack length. A summary of crack size estimations from the UT and ECT examinations performed on Scoping Specimen 7 is provided in Table 4-2. For this flaw, the estimated aspect ratio ranges from 7.7:1 to 9.2:1.

Optical profilometry measurements were performed on the crack in Scoping Specimen 7 to determine the COD. Gray-scale images with annotations of COD measurements are provided in Figure 4-17. These measurements indicate a COD of < 10 µm and is considered typical along the entire length of the crack.

Table 4-2. Summary of Scoping Specimen 7 crack size estimations obtained from UT and ECT measurements.

	Depth Estimate	Length Estimate
UT (Automated half-V)	39% through-wall 4.9 mm (0.193 in.)	45 mm (1.77 in.)
ECT	---	38 mm (1.48 in.)
Estimated aspect ratio – 7.7:1 to 9.2:1 Destructive Analysis was not performed on Scoping Specimen 7		

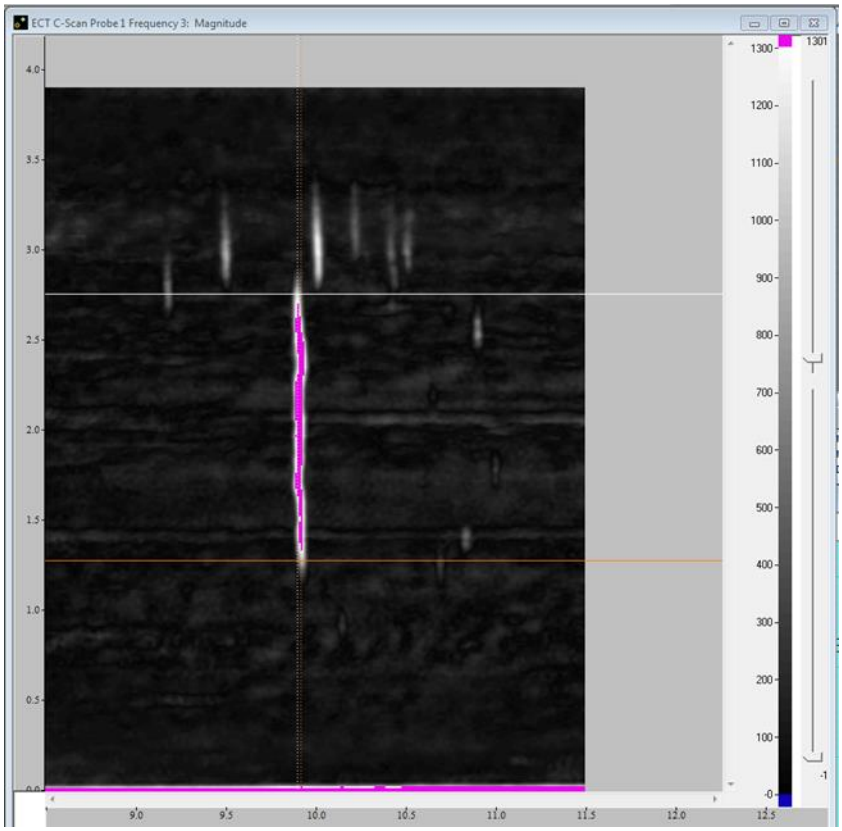

Figure 4-16. ECT examination response image for scan of Scoping Specimen 7 at 750 kHz.

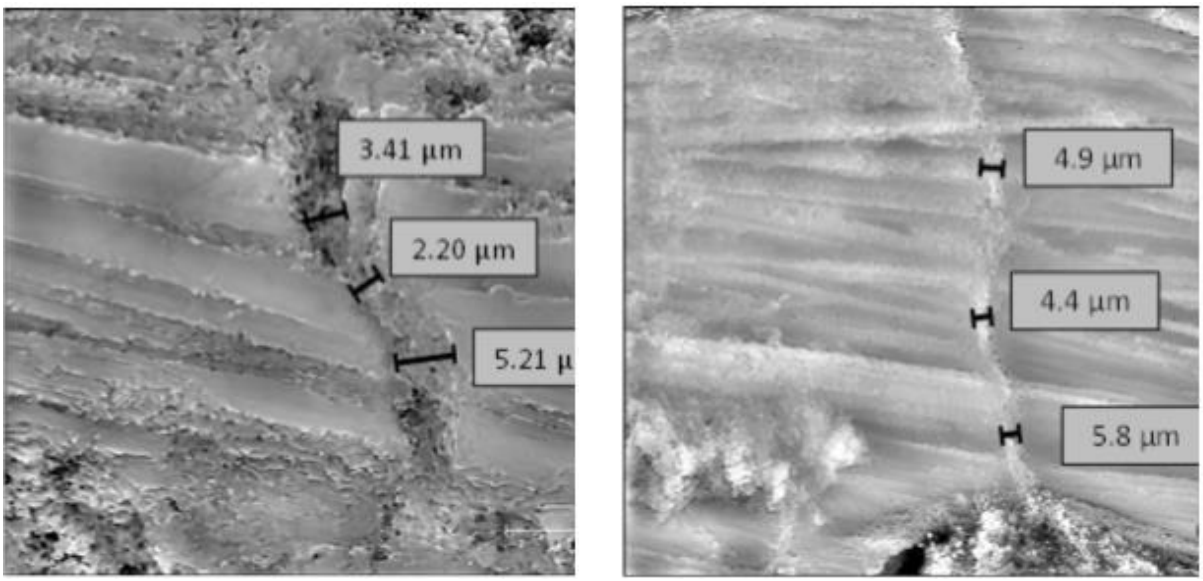

Figure 4-17. Optical profilometry images of Scoping Specimen 7 crack opening in two locations. Measurements of COD are indicated.

4.4 Characterization of Scoping Specimen 8

Scoping Specimen 8 was prepared with a high-temperature mask with a 12.5 mm (0.5 in.) linear penetration made to obtain a desired 2:1 aspect ratio. ECT characterization was performed post-test after removal of the mask to verify the length of crack formed. In addition, both manual and automated UT were performed to estimate the depth of the crack. The response image obtained from ECT scanning of Scoping Specimen 8 is included in Figure 4-18 and the response images obtained from half-V automated UT examination are included in Figure 4-19. The C-scan image shows some secondary indications, likely caused by the initiation of smaller cracks. A summary of crack size estimations from the UT and ECT examinations performed on Scoping Specimen 8 is provided in Table 4-3. From the summary table, it is evident that the manual UT resulted in much larger estimations of crack size than automated UT. Manual UT was performed by full-V examination with the specimen in the test rig and with load applied, which held the crack open. The automated UT measurements were performed after removing the test specimen from the test rig. A full-V examination was unable to identify a tip signal, which resulted in the half-V sizing attempt (Figure 4-19). The discrepancy between the manual UT and automated UT results motivated destructive analysis of Scoping Specimen 8 to confirm the flaw size. An approximate measurement of the crack dimensions using calipers indicated a crack depth of 7.6 mm (0.3 in.) and crack length of 25 mm (1.0 in.). These measurements are in closer agreement with the results of the manual UT measurements, which indicate the crack aspect ratio is 3.1:1.

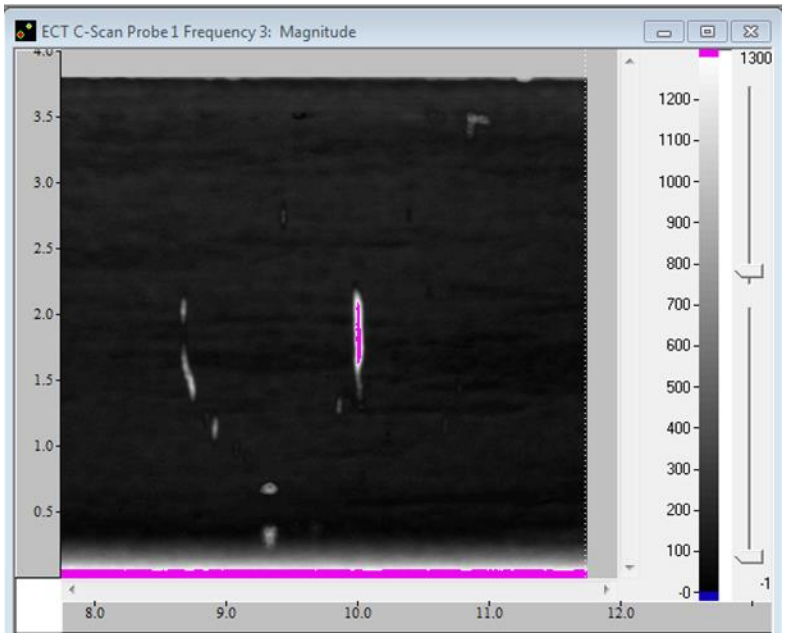

Figure 4-18. ECT examination response image for scan of Scoping Specimen 8 at 750 kHz.

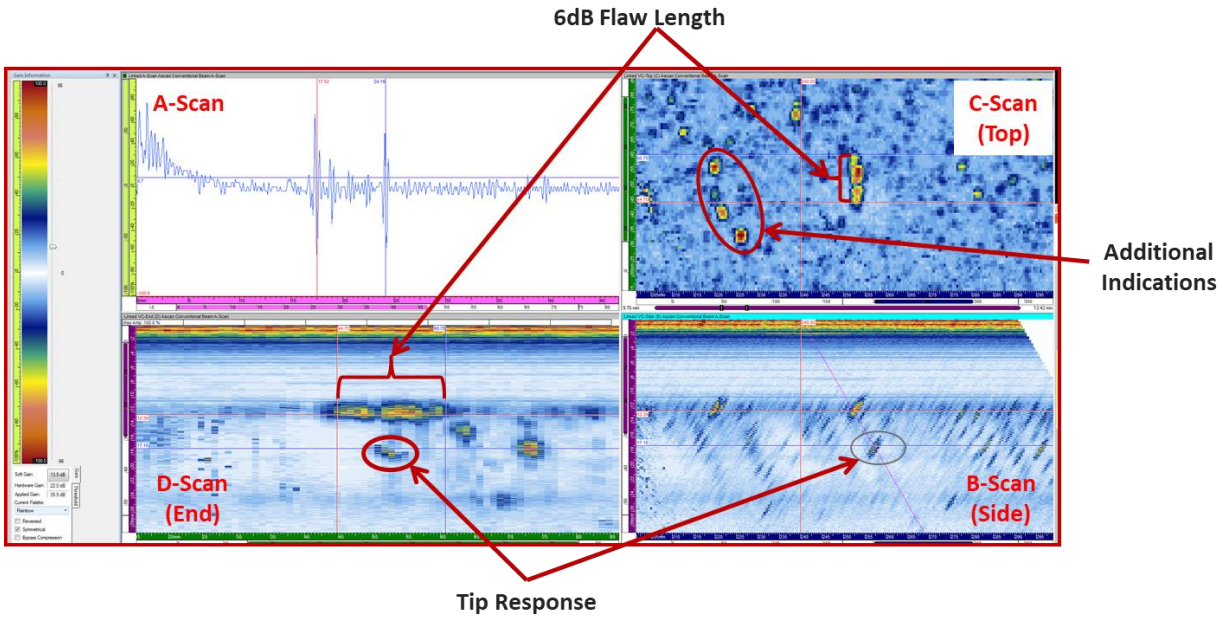

Figure 4-19. Automated UT examination response images for scan of Scoping Specimen 8 (*top left*: A-scan, *top right*: C-scan, *bottom left*: D-scan, *bottom right*: B-scan).

Table 4-3. Summary of Scoping Specimen 8 crack size estimations obtained from UT and ECT measurements and Destructive Analysis.

	Depth Estimate	Length Estimate
ECT	---	14 mm (0.54 in.)
UT (Automated half-V)	37% through-wall 4.8 mm (0.19 in.)	16 mm (0.63 in.)
UT (manual full-V)[(a)]	73% through-wall 9.4 mm (0.37 in.)	29 mm (1.15 in.)
Destructive Analysis	60% through-wall 7.6 mm (0.3 in.)	25 mm (1.0 in.)

Estimated aspect ratio – 3.1:1 (based on manual UT data)
(a) Manual UT was performed with the specimen in the test rig and with load applied, which held the crack open.

4.5 Characterization of NDE Specimen 1

NDE specimen 1 was characterized by UT and ECT examination. This specimen had a mask applied with a 12.5 mm (0.5 in.) long linear penetration to achieve a smaller aspect ratio, as was done for Scoping Specimen 8. The ECT response image obtained for the test specimen at 800 kHz is shown in Figure 4-20. The length of the crack is estimated to be 12 mm (0.48 in.) based on the eddy current response. Both half-V and full-V automated UT examinations were also performed on the specimen. A photograph of the specimen undergoing automated UT examination is provided in Figure 4-21 and the response images obtained from the half-V examination are included in Figure 4-22. A flaw tip signal for the primary crack could not be identified in any response images indicating that the flaw is of shallow depth (approx. 2–3 mm or less). The C-scan image shows some secondary indications, likely caused by the initiation of other small cracks. Thus, this specimen can be useful in testing the ability of NDE technologies to detect

cracks at early stages of growth and distinguishing technologies that exhibit exceptional detection and depth sizing capabilities. A summary of the crack size estimations based on UT and ECT measurements is included in Table 4-4.

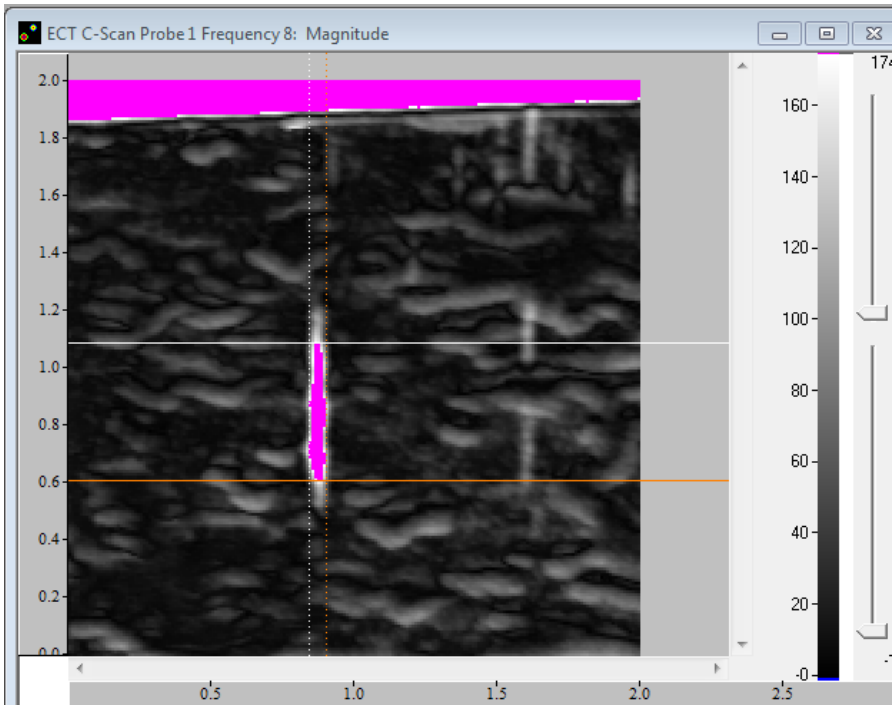

Figure 4-20. ECT examination response image for scan of NDE Specimen 1 at 800 kHz.

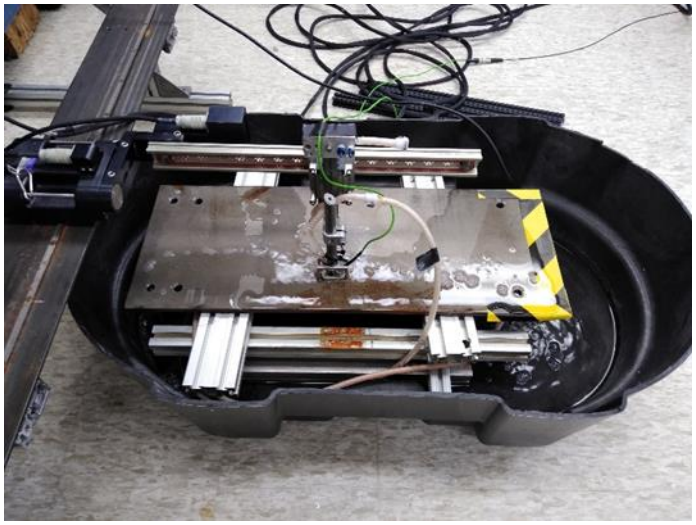

Figure 4-21. Photograph of automated UT examination of NDE Specimen 1.

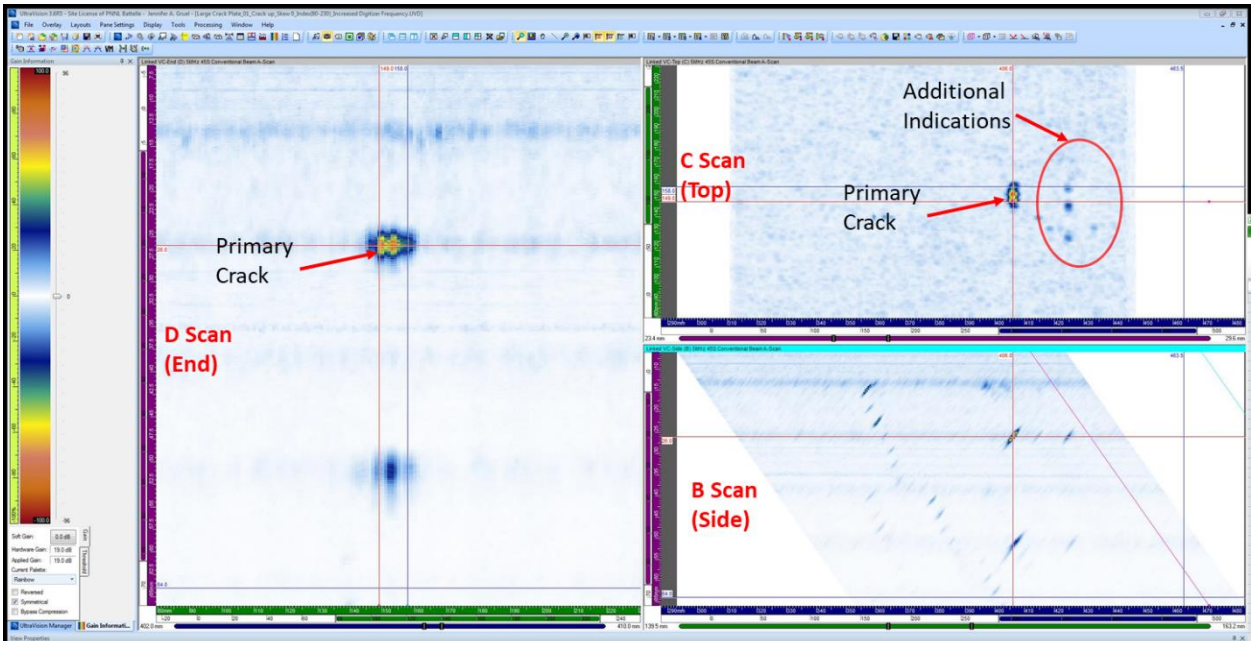

Figure 4-22. Automated UT examination response images for scan of NDE Specimen 1 (*left*: D-scan, *top right*: C-scan, *bottom right*: B-scan).

Table 4-4. Summary of NDE Specimen 1 crack size estimations obtained from UT and ECT measurements.

	Depth Estimate	Length Estimate
ECT	---	12 mm (0.48 in.)
UT (Automated half-V and full-V)	---	11 mm (0.43 in.)
Destructive Analysis was not performed on NDE Specimen 1		

4.6 Characterization of NDE Specimen 2

NDE Specimen 2 was characterized by automated UT examination. The UT scanning was performed for angles of 45°, 60°, and 70° for both half-V and full-V paths. A photograph of the specimen undergoing automated UT examination is provided in Figure 4-23 and the response for the 45° half-V path examination is displayed in Figure 4-24. The average flaw depth estimated from the automated UT examinations is approximately 8 mm (0.31 in.) and is reported in Table 4-5. This specimen was not examined by ECT, but an average length of the crack was estimated as 42 mm (1.65 in.) based on the automated UT examination responses.

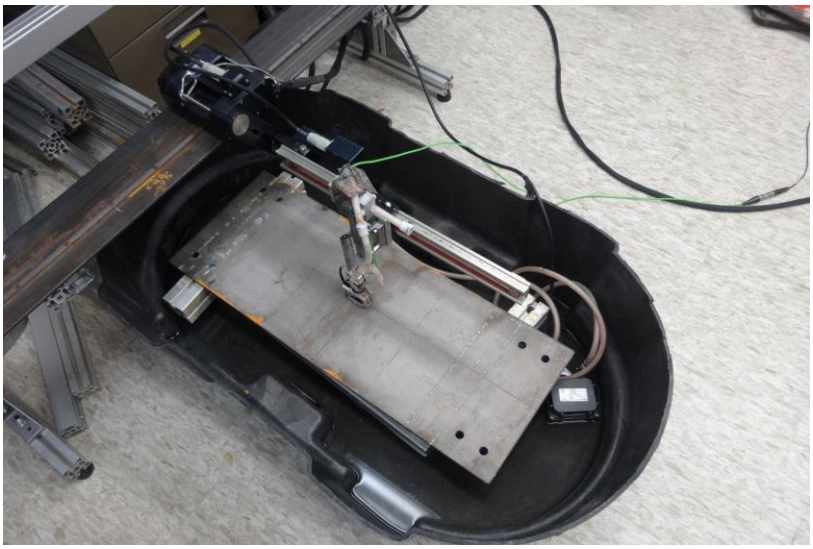

Figure 4-23. Photograph of automated UT examination of NDE Specimen 2.

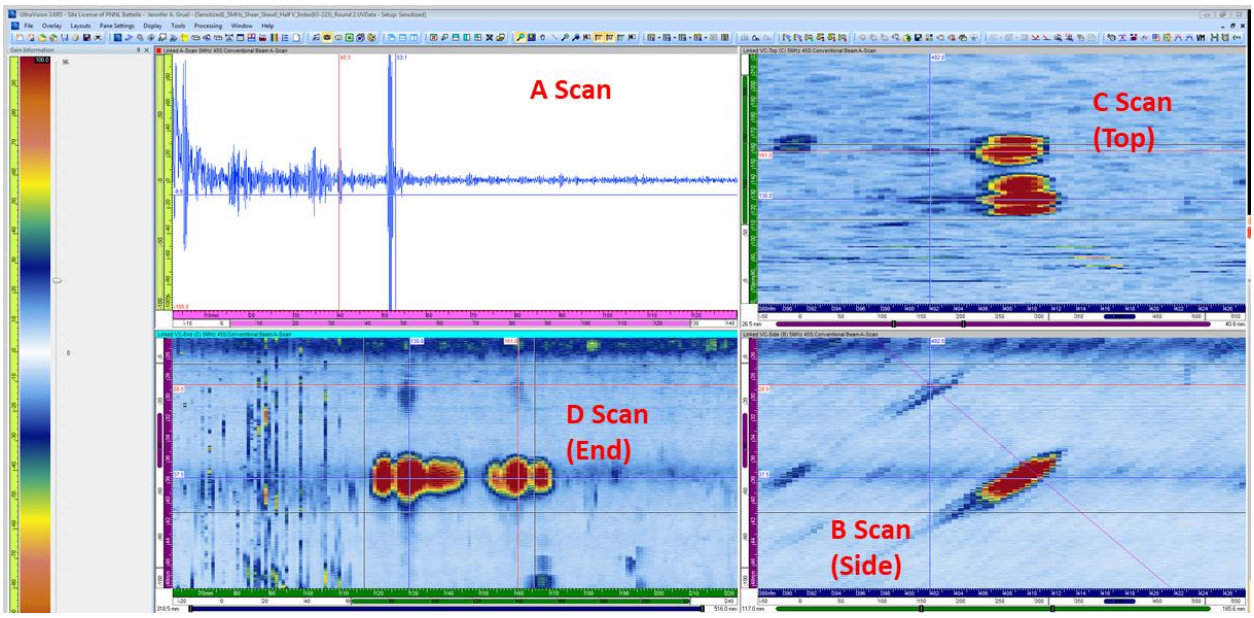

Figure 4-24. Automated UT examination response images for scan of NDE Specimen 2 (*top left*: A-scan, *bottom left*: D-scan, *top right*: C-scan, *bottom right*: B-scan).

Table 4-5. Summary of NDE Specimen 2 crack size estimations obtained from UT measurements.

	Depth Estimate	Length Estimate
UT (automated half-V and full-V)	62% through wall 8 mm (0.31 in.)	42 mm (1.65 in.)
Estimated aspect ratio = 5.25:1 Destructive Analysis was not performed on NDE Specimen 2		

5.0 Conclusions and Recommendations

This report describes the "cook-and-look" approach for fabricating SCC flaws in stainless-steel NDE specimens. The four-point bend method was used to apply load to specimens, and a cup containing $MgCl_2 \cdot 6H_2O$ solution was brought into contact with the specimen at the location of maximum stress. The $MgCl_2 \cdot 6H_2O$ solution was heated to near or at boiling temperatures. The scoping phase helped identify practical improvements to the test setup and suitable test parameters for initiating and growing cracks with a range of through-wall depths in time intervals of 1 week or less.

Practical improvements identified through the scoping phase included:

- Replacing the PVC cup for the $MgCl_2 \cdot 6H_2O$ solution with a CPVC cup
- Reorienting the test rig so that the $MgCl_2 \cdot 6H_2O$ solution contacted the specimen from the side instead of from underneath
- Replacing the original polyamide mask material with a high-temperature engine enamel
- Adjusting the length of the mask penetration to control crack aspect ratio.

Suitable test parameters identified through the trial-and-error scoping phase are:

- Sensitizing the 304 stainless-steel specimens by soaking in a furnace for 40 hours at 600°C
- $MgCl_2 \cdot 6H_2O$ solution concentration of 6 mol/L or greater
- $MgCl_2 \cdot 6H_2O$ solution heated to 108°C.

By the end of the scoping phase, the ability to generate cracks with depths that ranged from 25% to 75% of the plate thickness and with small COD (approx. 10 µm) was demonstrated. Also, an ability to control the location of crack initiation was achieved by the application of the high-temperature enamel mask. Finally, an ability to control crack aspect ratio was shown through modification of the length of penetration through the mask.

Two NDE specimens were fabricated following the scoping phase of testing. The first NDE specimen was cautiously removed after a day of exposure to examine crack formation. An automated UT examination was unable to identify a crack tip signal suggesting the flaw is shallow (< 2 mm–3 mm). As is, this specimen can be useful in testing the ability of NDE technologies to detect cracks at early stages of growth and distinguishing technologies that exhibit exceptional detection and depth sizing capabilities. A second NDE specimen was fabricated to grow a larger crack. In this case, the specimen was initially exposed for 30 hours and exposed again for another 24 hours. Following these exposures, a crack with depth of 8 mm (0.31 in.) was observed and estimated based on automated UT measurements.

The testing performed in these efforts focused on specimens consisting only of base material. In the field, the concern with CISCC is focused on the HAZ near welds. A potential follow-on step to these efforts is to fabricate flaws in welded specimens.

6.0 References

ASME. 2017. *ASME Boiler and Pressure Vessel Code - An International Code*, NY: American Society of Mechanical Engineers.

Cumblidge SE, SR Doctor, PG Heasler and TT Taylor. 2010. *Results of the Program for the Inspection of Nickel Alloy Components*. NUREG/CR-7019; PNNL-18713, Rev. 1. Washington, DC: U.S. Nuclear Regulatory Commission.

EPRI. 2016. *Dry Canister Storage System Inspection and Robotic Delivery System Development*. Report 3002008234. Palo Alto, CA: Electric Power Research Institute.

EPRI. 2017a. *Inspection and Delivery System Development and Field Trials for Dry Canister Storage System Evaluation*. Report 3002010621. Palo Alto, CA: Electric Power Research Institute (EPRI).

EPRI. 2017b. *Extended Storage Collaboration Program (ESCP): Nondestructive Evaluation Subcommittee – Industry Progress Report*. Report 3002010617. Palo Alto, CA: Electric Power Research Institute (EPRI).

Meyer R, A Pardini, J Cuta, H Adkins, A Casella, A Qiao, MR Larche, A Diaz and SR Doctor. 2013. *NDE to Manage Atmospheric SCC in Canisters for Dry Storage of Spent Fuel: An Assessment*. PNNL-22495. Richland, WA: Pacific Northwest National Laboratory. ADAMS Accession No. ML13276A196.

Meyer RM and PG Heasler. 2017. *Results of Blind Testing for the Program to Assess the Reliability of Emerging Nondestructive Techniques*. NUREG/CR-7235, PNNL-24196. Washington, DC: U.S. Nuclear Regulatory Commission. ADAMS Accession No. ML17159A466.

NRC. 2012. *Potential Chloride-Induced Stress Corrosion Cracking of Austenitic Stainless Steel and Maintenance of Dry Cask Storage System Canisters*. NRC Information Notice 2012-20. Washington, D.C.: U.S. Nuclear Regulatory Commission. ADAMS Accession No. ML12319A440.

NRC. 2014. *Identification and Prioritization of the Technical Information Needs Affecting Potential Regulation of Extended Storage and Transportation of Spent Nuclear Fuel*. Washington, DC: U.S. Nuclear Regulatory Commission. ADAMS Accession No. ML14043A402.

NRC. 2016. *Standard Review Plan for Renewal of Specific Licenses and Certificates of Compliance for Dry Storage of Spent Nuclear Fuel*. NUREG-1927, Rev. 1. Washington, DC: U.S. Nuclear Regulatory Commission. ADAMS Accession No. ML16179A148.

NRC. 2019. *Managing Aging Processes In Storage (MAPS) Report*. NUREG-2214. Washington, DC: U.S. Nuclear Regulatory Commission. ADAMS Accession No. ML19214A111.

Pacific Northwest
NATIONAL LABORATORY

www.pnnl.gov

902 Battelle Boulevard
P.O. Box 999
Richland, WA 99352
1-888-375-PNNL (7665)

Prepared for the U.S. Nuclear Regulatory Commission
under a Related Services Agreement with the U.S. Department of Energy
CONTRACT DE-AC05-76RL01830

U.S. DEPARTMENT OF
ENERGY